Deliverable 9.8

Report on mobile battery test platform and results of the measurements

Prepared by:

Kim Winther, DTI
kwi@dti.dk
Morten Holst, DTI
mhj@dti.dk

Date: **December 18th, 2014**

Version: **4.1**

Document Information

Authors

	Name	Company
Key author	Kim Winther	DTI
Further authors	Morten Holst	DTI

Distribution

Dissemination level		
PU	Public	x
PP	Restricted to other programme participants (including the Commission Services)	
RE	Restricted to a group specified by the consortium (including the Commission Services)	
CO	Confidential, only for members of the consortium (including the Commission Services)	

Revision history

Version	Date	Author	Description
1.0	August 8th, 2014	Kim Winther	Initial version
2.0	November 12th, 2014	Morten Holst	Thorough draft
3.0	November 26th, 2014	Morten Holst	Final version
4.0	December 17th, 2014	Luis de Prada	External Review
4.1	December 18th 2014	Kim Winther	For Approval

Status	
For Information	
Draft Version	
Final Version (Internal document)	
Submission for Approval (deliverable)	X
Final Version (deliverable, approved on)	

Table of Contents

List of Figures

List of Tables

List of Abbreviations

AC	Alternative Current (electricity grid)
BMS	Battery Management System
CA	Consortium Agreement
CAN	Controller Area Network
CHAdeMO	"CHAdeMO" is an abbreviation of "CHArge de MOve", equivalent to "charge for moving", and is a pun for "O cha demo ikaga desuka" in Japanese, meaning "Let's have a tea while charging" in English
DC	Direct Current
DoW	Description of Work (Annex I of Grant Agreement)
EIS	Electric Impedance Spectroscopy
ESR	Equivalent Series Resistance
ESX	Equivalent Series reactance
EV	Electric vehicle
EVPC	Electric Vehicle Power Characterization
IPR	Intellectual Property Rights
ISO	International Organization for Standardization
OCV	Open-Circuit Voltage
OBD	On-Board Diagnostics
OBC	On-Board Computer
OEM	Original Equipment Manufacturer
PWM	Pulse Width Modulation
SOC	State of Health
SOH	State of Charge
SORDS	Standardized On-Road Driving Scheme
TNM	TÜV NORD Mobilität
WP	Work Package

1 Executive Summary

In this report, we investigate the performance of electric vehicle batteries and how that performance degrades over time. Battery degradation is a cause for great concern because batteries are the single most expensive part of the electric vehicle. The potential cost of replacing batteries therefore has a dramatic impact on the business case, both for the consumer and for the operators of charging infrastructure.

Monitoring the performance of EV batteries requires a technical platform that allows electrical tests to be performed on the vehicles. It also requires knowledge about the impacts of temperature etc. on the batteries which may reduce capacity but are not the result of wear. Last but not least, it requires a set of well-defined performance metrics.

In that context, the main outcomes of the analysis presented in this report are:

- **Technical test platform:** By equipping a dedicated Battery Service Vehicle with electrical load banks, AC/DC chargers, power analysers etc. the team developed a flexible, mobile test platform that was used both in laboratories and in the field to analyse the state of EV batteries.
- **Well-defined performance metrics**: We found that neither the Battery Capacity, nor the State of Health nor the State of Charge were universally defined. Thus these important performance metrics can be used in a somewhat arbitrary way.
- **Access to batteries**: We found that direct access to the battery poles on modern EV's is hindered by a complex set of control functions. Thus a simple plug-and-play approach to battery testing was not possible. Instead we used the vehicle itself as a test mule and recorded the necessary data from the CAN bus.
- **Advanced modelling**: To simulate the impact of load profile on the performance of the batteries a Randle's circuit modelling was used. This allowed standardised test sequences like ISO12405-2 to be simulated without taking the battery out of the car.
- **Impacts of temperature**: We found a significant impact of temperature on the available energy capacity of the batteries. This underlines our observation that battery measurements are highly subject to influence by the weather.
- **Performance over in-use life time**: Despite doing many tests in laboratories and in the field we found **no proof of irreversible degradation** over the time span of the project. One battery did break down at the age of 4 years, but even this was relatively easily repaired. Our tests confirmed that the battery performed as new after the repair.

2 Introduction

This report deals with periodic battery capacity measurements (local and mobile test) on electric vehicles used in the project.

2.1 Purpose and background

During a large EV demonstration program it is a prerequisite for close observation of battery deterioration that periodic battery capacity measurements are conducted. When considering a large EV demonstration fleet, the cost and inconvenience of transporting each vehicle to a laboratory facility in order to conduct battery test can be significant. For this reason, a mobile battery test platform was set up which enables local onsite battery capacity testing.

The mobile test platform is a multipurpose van prepared with custom interior for accommodating a complete set of test equipment for batteries and electric vehicles. This includes a set of electrical load banks and chargers for capacity measurements and equipment for more sophisticated measurements. The mobile test platform was successfully used for both the test in the field and some of the testing in the lab.

An international standard ISO12405-2 (High Energy Application, chapter 7 Performance tests) was published in 2012 by ISO/TC22/SC21. This standard however requires separation of the battery pack from the vehicle. This is not feasible for on-site testing because batteries are nowadays highly integrated into the vehicles. Instead the principles of pulse power characterization profile, internal resistance calculation, standard charge cycle etc. was used with the battery in place.

Capacity measurements have been done at various levels in the intervals 0.20-0.84 C for discharge, 0.07-0.14 C for charge, along with a number of pulse discharges to find the internal resistance of the battery pack. The specific procedure for the capacity measurement was in practice dependent on a number of practical issues.

The original intention was to include 20-30 vehicles and test these vehicles 2-4 times giving a total of 60-100 battery tests. The number of vehicles available for test was however much smaller due to limited availability of vehicles from the demo regions. To obtain a sufficiently large number of measurements we added a number of loaned and leased vehicles. In total there were 2-6 vehicles available for test on 3 occasions. The available vehicles were tested several times to increase the amount of data. We also included data from our own vehicles. In full we obtained about 61 capacity readings. To get sufficient data for SOH evaluation, a remote SOH reading was used in cooperation with Renault giving readings on 16 vehicles registered in Denmark.

For battery exchange stations and intelligent charge systems it is pivotal that the lifetime and actual SOH of the batteries are monitored closely, in order to provide an overview of the actual battery capacity of a given EV fleet. Therefore batteries from the demonstration fleet vehicles have been tested and analysed experimentally and subjected to a capacity degradation analysis.

By coupling key experimentally obtained parameters with a validated model, we have demonstrated that a battery SOH estimation can be based on non-intrusive methods.

The possibility of using modelling and advanced measurement techniques, such as AC impedance spectroscopy, for determination of battery SOH has been investigated. Although most vehicles have safety and control systems preventing such actions we found useful to demonstrate the potential of such techniques. Therefore a demonstration measurement was carried out on a specially prepared vehicle.

These tests have provided some useful information to the future development of SOH models.

2.2 Important definitions

Before beginning any effort to measure and evaluate performance of batteries it is necessary to be very clear about the definitions of battery performance.

2.2.1 What is Capacity?

When buying a new battery, it typically has a label on it with the rated capacity, the so-called nominal value. This number originates from the capacity value of which the battery was designed to have, including production tolerance. Maybe the manufacturer did also specify a guaranteed minimum capacity value of the battery.

Capacity of a battery is by engineers defined as the amount of Ampere-hours in a battery, not including any voltage information. The actual required information at the user end is the amount of kilowatt-hours (energy) that can be discharged from the battery. Therefore, we define *energy capacity* measured in kWh. Capacity depends on the rate of discharge, temperature and for lithium-ion batteries it has strict voltage bounds.

Additionally, capacity degrades with the ageing of the battery (see Figure 2.2.1).

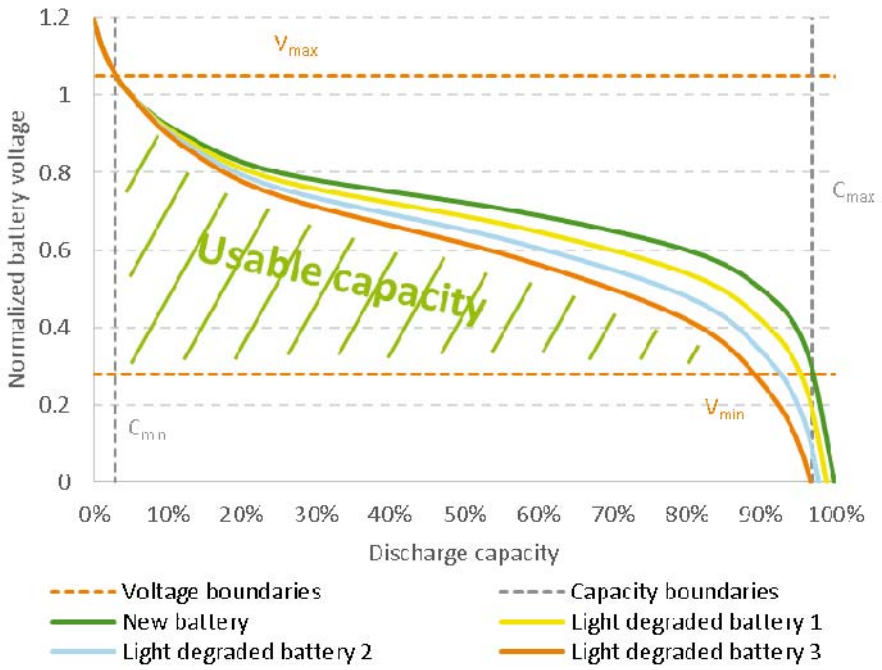

Figure 2.2.1: Capacity and degradation explained

The actual storage “volume” of the battery can never be measured physically. It can only be estimated by discharging a fully charged battery under given conditions and then giving a prediction under any given future conditions. Even the battery’s own management system cannot know the exact capacity or actual energy content of the battery, but from experience an algorithm can be designed to estimate the SOH and the current SOC of the battery.

The original definition of battery capacity was probably based on the first battery types, which had the electrical current drawn with little concern about the decreasing state of voltage during discharge. With today’s common battery type, Lithium-Ion, the end-of-discharge criterion is defined by a strict voltage limit defined by the manufacturer of the battery and possibly the manufacturer of the EV. The EV manufacturer has the degree of freedom to reduce the battery energy content available to the driver within the battery management system, for instance in order to provide a more uniform perception of the battery performance.

It is known that the ambient conditions influence the battery performance, but the exact magnitude of this relationship has not been fully quantified yet. Therefore, if an ambient condition increases the internal impedance, the voltage will be lower, hence not only the energy capacity (kilowatt-hours) of the battery is decreasing, but it is suddenly plausible that the charge (Ampere-hours) released by the BMS is no longer constant.

2.2.2 What is state of health?

State of health (SOH) is an arbitrary figure of merit, which cannot be expressed in exact quantitative terms.

Vehicle manufacturers use different ways of expressing SOH. An example is show in Figure 2.2.2 and Figure 2.2.3.

Figure 2.2.2 SOH indicator on a Nissan Leaf

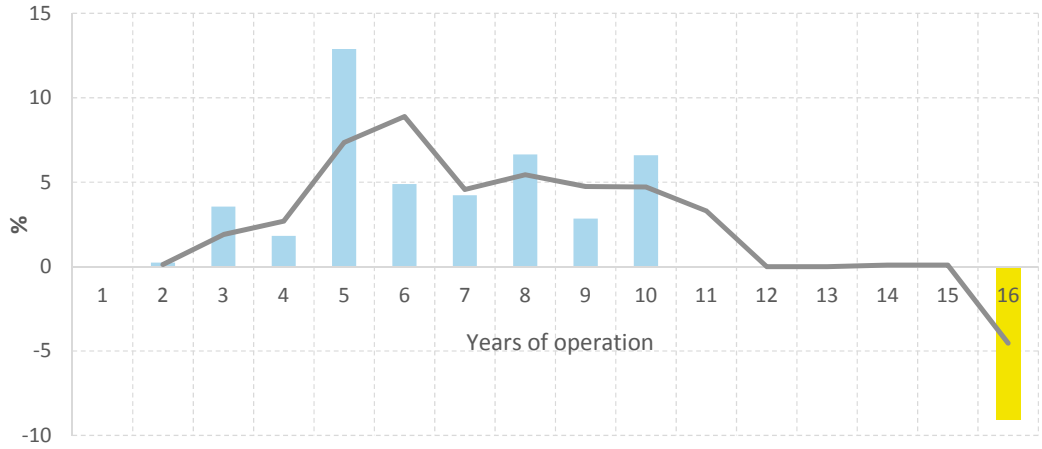

Figure 2.2.3: Degradation data obtained from a fleet of Renault Zoe vehicles

The definition of the battery state of health has not been standardized and therefore, for the sake of regularity, a local definition is brought here. When a lithium-ion battery degrades, it can generally be measured in two terms; capacity fade and rise of internal impedance.

The actual state of health of a battery is its discharge energy capability at the time being, hence the energy capacity. The energy capacity of a used battery includes an amount of degradation, which has to be subtracted from the initial capacity.

Our version is a complex compilation of impedance (expressed in Nyquist plot), OCV and r-factors (ISO 12405-2) compared to a new battery.

2.2.3 What is State of Charge?

State of charge (SOC) is, actually, also kind of arbitrary since it is by definition the ratio of the electrical energy available to be discharged and the total capacity of the battery. However, the total capacity is defined by the manufacturer, not measured so there could be different values stated for the same battery, if the manufacturer decides so. Furthermore, the electrical energy to be discharged will depend on the discharge current, high current will increase losses and that is not controlled by the battery. So actually SOC is only an estimate.

2.2.4 What is Impedance?

Any flow of energy through a battery is met with some kind of resistance. This internal battery resistance, is not a single and constant value. In the simplest possible way this resistance can be compared to the shock absorber in a car. The shock absorber resists movement with a force (i.e. voltage drop) that is directly proportional to the speed of movement (i.e. the current).

However, in the real world batteries are more complex than that. The response of a battery is also time-dependent, so that the response is not instantaneous. If current is applied to the battery the voltage rises gradually to a stable level. When the current stops the voltage returns gradually to a new level.

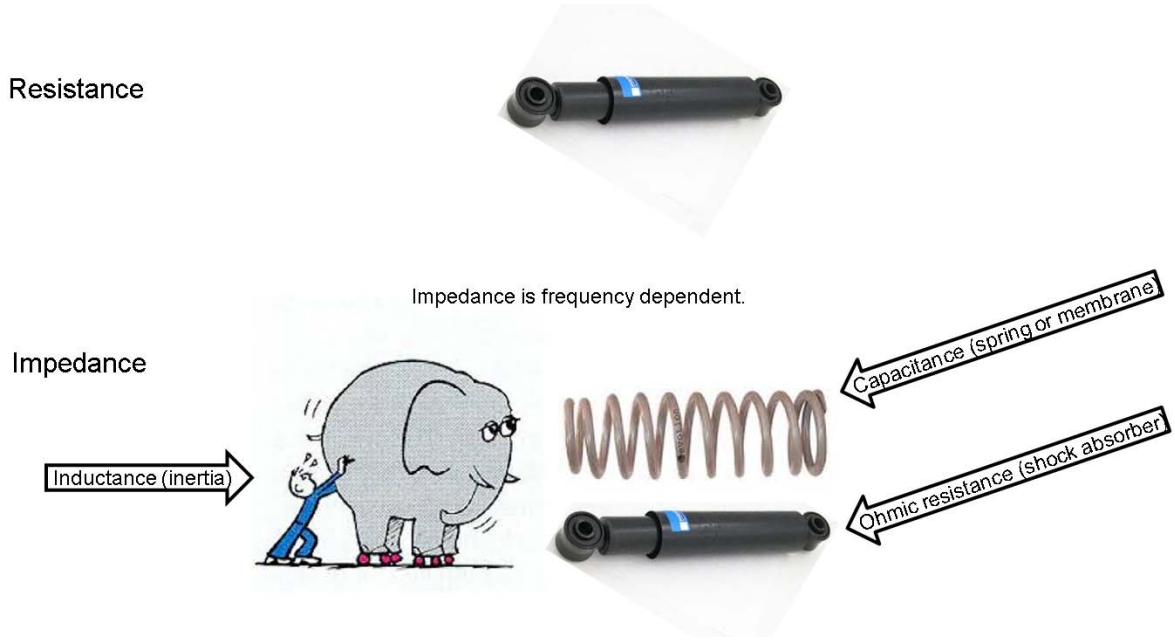

Figure 2.2.4: Impedance explained

2.3 Battery types used in this project

The primary battery technology used in EVs is a branch of the Lithium-Ion type. The chemistry is typically cobalt, nickel, manganese or a combination of these.

The batteries are somehow divided into smaller modules of a few battery cells configured in series and parallel connection. The modules are stacked in a series connection until the desired pack voltage is reached. An EV can contain more than one battery pack, but the stack of modules can also be divided into partial packs in series connection having different physical locations in the EV body.

In northern countries the climate is rather cold and very low temperatures (below -5°C) can be expected in the wintertime, where the EV battery should be held warm, but a few days or weeks with high temperatures (above 25°C) can still be expected in the summertime. Therefore, an EV in the northern region should be equipped with a battery climate control to regulate the battery temperature both up and down. The climate control can be direct-air or water-borne designed to fit the climate region where the EV is sold.

EV	Number of cells	Nominal voltage	Nominal capacity	Chemistry	Cooling type
Nissan Leaf	192	365 V	24 kWh	LMO-NCA	Passive
Renault Fluence ZE		400 V	22 kWh	NMC-LMO	Air
Mitsubishi i-MiEV	88	330 V	16 kWh	LMO-NMC	Air
Tesla Model S	7104	346 V	85 kWh	NCA	Water
Fiat Fiorino Micro-Vett		380 V	31 kWh	LNMCO	None
Fiat Fiorino Enerblu	72	267 V	20 kWh	LCO	None

Table 2.1: Details about battery types used

3 Battery performance evaluation

This part of the report contains information about the mobile test platform, the battery simulations and the results.

3.1 Mobile test platform

The mobile test platform has been built up around the base vehicle. The vehicle equipment is optimized to be able to work the longest possible time in waste land without any access to the mains supply. Therefore, the vehicle has its own power plant, an 11kW gasoline-powered generator and a power inverter that transforms 12V DC to 230V AC. Please see Figure 3.1.1.

Figure 3.1.1: The mobile test platform delivered at DTI grounds in Aarhus, Denmark

The main reason to bring a power generator set is to be able to recharge an empty EV battery in the waste land. Please see Figure 3.1.2. The vehicle is equipped with two kinds of EV chargers – a 3kW AC mode 3 and a 20kW DC CHAdeMO mode 4. The DC-charger is actually able to provide 20kW of so-called EV quick charge or fast charge, but including the losses in the charger, the actually DC charging power is limited to 8kW by the power generator.

To acquire EV battery information combined with driving information, the vehicle is equipped with different kinds of CAN dataloggers, including non-intrusive inductive sensors, so-called CAN-click, that read CAN information without dismantling wires. In addition to this, you shall find various meters in the vehicle to measure voltage, current, power and temperature.

Figure 3.1.2: The mobile test platform in action on proving grounds in Karup, Denmark

A compact laptop has been built onto a battery energy storage, which extends the laptop operating time. A wireless network of sensors communicates with this laptop through a gateway built into the same case as the battery energy storage. The sensors can measure different types of voltage signals, including current signals, which are transformed into voltage by hall-element transducers. Other types of battery energy storages are available to power any auxiliary equipment.

The vehicle brings its own weather station to the proving grounds, wherefrom the local status of air temperature, wind, pressure etc. can be logged.

An automobile trailer is brought along to carry a vehicle, for example a troubling EV with a flat battery. The trailer also serves as a mule, if the number of vehicles to drive exceeds the number of available drivers. Please see Figure 3.1.3.

Figure 3.1.3: Mobile test platform in action on proving grounds in Værløse, Denmark

Different types of energy meters and cable adaptors ensure that all EVs can be charged and measured upon charging almost everywhere. The vehicle carries isolated hand tools and safety gear to be used when working in areas with live voltage of the EV battery.

A meter-measuring wheel and traffic cones are used to form a test track. A tent, table and chairs are all auxiliary equipment, when testing vehicles in the field. The vehicle is also equipped with a diesel-fuel furnace and workspace to sit in the back of the vehicle, when stationary.

A mobile, water-cooled DC load bank has been built to perform controlled discharge tests on EV batteries anywhere, if there is physical access to the high voltage terminals.

If a detailed AC power analysis is needed, the vehicle does also have equipment for this.

A detailed overview is shown in Table 3.1 below.

Component	Manufacturer	Type or model	Specifications
Base vehicle	Daimler	Mercedes Vito	Diesel, 2.2 CDI with air rear suspension
Power generator set	Europower Generators	EP16000TE	Gasoline, 15 kW
DC charger	EVTEC	MobileFastCharger	CHAdeMO, mode 4, 20 kW
AC charger	Schneider Electric	EVLink 3kW	Mode 3
CAN datalogger with GPS	Racelogic	VBOXII SX10	10 Hz
CAN datalogger with GPS	Racelogic	VBOXII Micro	10 Hz
Datalogger with GPS	Racelogic	Performance Box	10 Hz
Non-intrusive CAN read-only sensors	Vikingegaarden	CAN click	
Current clamp meter	Fluke	i1010	For use with multimeter
Power clamp meter	Fluke	PQ 345	3 phase symmetric AC and DC
Electricity clearing meter	Kamstrup	685-382-SK10	3 phase AC
Logging power meter	Power Detective		1 phase AC, 5 pcs.
Multimeter	Fluke	376	
Multimeter	Fluke	289/FVF	
Flexible current probe	Fluke	i3000 FLEX-24	For use with multimeter
Wireless sensors	National Instruments WSN	3202 and 3226	Voltage and temperature
Differential probe for high voltage	Hameg	HZ115	For use with multimeter, 0-1000V
Current transducer	LEM	50, 100 and 400	
Weather station	Davis	Vantage Vue	
Temperature datalogger	Testo	176T4	4 channel
Automobile trailer	Variant	Flatbed with ramps	3,000 kg
12V jumpstarter			12V

Isolated handtools and safety gear	CIMCO		
230V power inverter	Waeco	Sine Power MSP1012	
Travel laptop	HP	Elitebook 2560p	
Battery energy storage for laptop	GWL Power		3x12V, 17Ah
Inkjet printer	Epson Stylus	SX445W	
Air compressor			
Power Analyzer	ZES Zimmer	LMG450	
Mobile DC load bank	TDI DC load and EA power supply	DTI-designed rack	
Supported charging plug standards	Type 1: SAE J1772-2009		1 phase AC
	Type 2: VDE-AR-E 2623-2-2 (Mennekes)		1 or 3 phase AC
	IEC 61851-1 Mode 4 (CHAdeMO)		DC
Power cable adaptors	CEE	Red colored	3 phase, 16 and 32A
	CEE	Blue colored "camping"	1 phase, 16A
	Schuko		1 phase, 13A
	DK 2-1a		1 phase, 13A
Communication adaptors	OBD CAN		
Meter measuring wheel	Gottlieb Nestle		
Traffic cones			28 pcs.
Fire extinguisher		CO_2	
Tent, table, chairs, coffeemaker			

Table 3.1: List of equipment for mobile test platform

3.1.1 Electro Impedance Spectrography

By recording a battery's response to an injected AC signal, it is possible to determine the internal impedance of the battery. Thus this is normally performed directly on battery cells, under controlled laboratory conditions, and not on EVs. In a battery pack, the impedance is much more complex. Firstly, the cells are configured in a grid with a number of cells in series and parallel – a pack value or an average cell value can be calculated back and forth. Secondly, the battery pack will always include parasitic components, like wiring, connectors, bus bars, contactors, fuses etc., which all inflict the total impedance, hence the average single cell impedance.

On advice from the OEMs it has been decided that EIS should not be used on EVs due to the heavy integration between the battery, BMS and vehicle control system. It is too complex to gain access to the EV battery. A correlation between EIS and SOH measurements would have been preferred.

Field EIS measurements have been attempted while driving on the road. However, it was not possible to obtain a stable response due to excessive electrical noise picked up by the voltage probe.

The project team have been looking for alternative methods, which resulted in the solution described in section 3.1.3.

3.1.2 CAN communication

All modern vehicles use CAN communication.

The current communication standards do not allow bidirectional flow of energy. In the near future however this is expected to change.

Some charging standards, like the CHAdeMO, use the CAN bus protocol to communicate.

The primary purpose of this communication is to perform safety interlock to avoid energizing the power connector before it is safe and to transmit battery parameters to the charging station. For example when to stop charging, target voltage, total capacity and how the charging station should vary its output current – the connected vehicle holds all this information.

The CHAdeMO standard requires integrated physical switches to work, which are capable of allowing energy to flow in both directions.

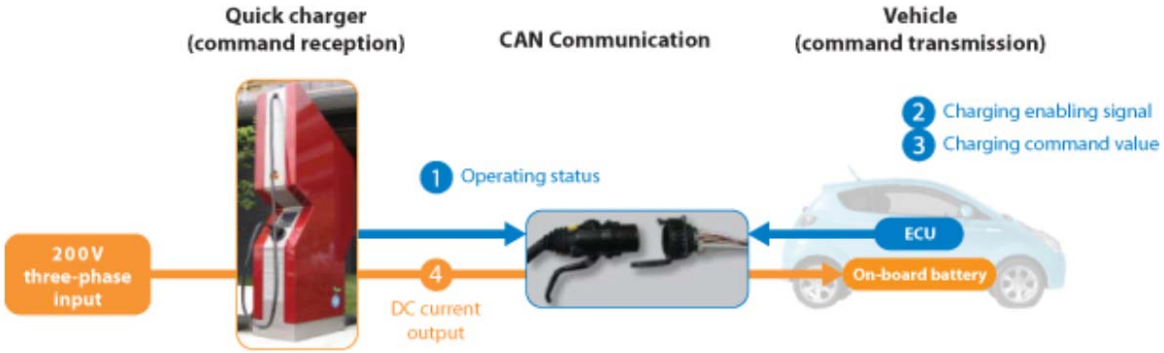

Figure 3.1.4: CAN communication as used in the CHAdeMO protocol

Other charging standards, like the SAE J1772-2009 or IEC 62196 Type 1, uses simple PWM and resistances to communicate. The EV sets a resistor depending on its status. The charging station detects a connected EV by putting out a 12V signal and measuring a certain voltage drop on another signal. If the circuit is open, no vehicle is connected. A 1 kHz square wave signal is used to test the protective earth system and to describe the available maximum current for charging by PWM modulation. At end-of-charge the station shifts the voltage signal to initiate a controlled shutoff prior to the actual disconnection of the power pins.

Simple electronics-based charging standards, like the SAE J1772-2009 or IEC 62196 Type 1, do not allow bidirectional energy flow.

For further explanation of CAN communication please see D6.1.

3.1.3 Non-intrusive methods

On advice from the OEM's it has been decided to use the vehicle itself as load bank. On newer EVs it is not possible to connect external load bank, e.g. to test in accordance to ISO 12405-2, due to the heavy integration between battery and vehicle control system. It is much more feasible to discharge the battery during a specified drive cycle, while monitoring the battery voltage and current non-intrusively via OBD, current clamps, Tesla owner's data logging and so-called CAN-clicks. Additionally, the Standardized On-Road Drive Scheme (SORDS) test was invented. For details please see Figure 3.1.5.

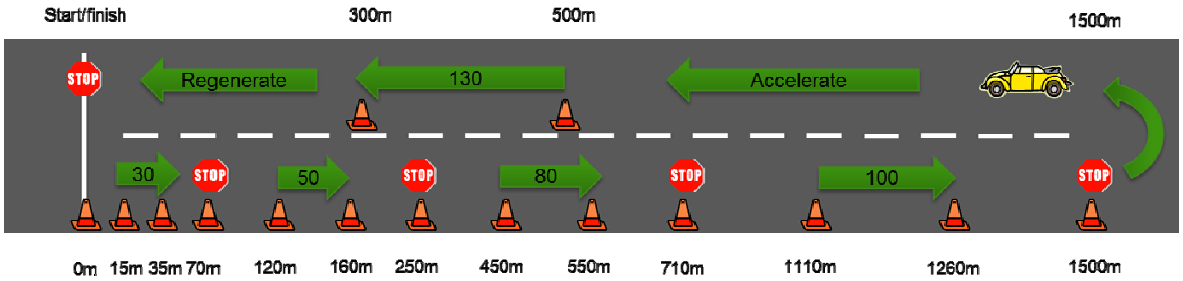

Figure 3.1.5: The SORDS drive cycle test scheme

Opening battery packs is a highly sensitive matter due to warranties, IPR etc. OEMs are not able to participate in open battery testing. Therefore, multiple battery packs cannot be expected available for open battery test. The goal is to obtain one single pack which must be bought at full price (Fiat Fiorino).

When going into the EV through the Type 1 or Type 2 connector, one hits the AC/DC charging device, which cannot be omitted without intruding the electrical system. Again, the CHAdeMO connector is interesting, because it uses DC power directly into the battery, except for contactors, fuses etc. A combined connector for both AC and DC charging exists, where the DC part is just as interesting.

Instead, an EV can easily be driven to give steep slopes in the battery power. The so-called step response from the battery during load step was recorded. The battery model was applied to these data in combination with the SORDS test data, yielding a sequence of impedance coefficients estimating the electrical inside of the EV system. From these coefficients a Nyquist plot can be drawn, just like with EIS, and the battery response to any type of discrete stimuli can be simulated.

3.2 Discharging through DC fast charge connector

A capacity measurement method relying on direct discharge of the battery independent of the vehicles drive train is desirable, as it can be performed fast and with less dependence on the ambient conditions compared to driving range based capacity estimations.

To track the decrease in capacity over time for a particular vehicle, a number of capacity measurements must be performed over an extensive period of time (for example every sixth month over a period of at least two years) to allow a noticeable degradation. Therefore, a mobile test setup which allows capacity measurements at a location convenient to the EV end-user is desirable.

A number of technical challenges must be dealt with to allow capacity measurement based on direct battery discharge.

These challenges are listed below and the way they have been resolved will be described in the following chapters. Subsequently, the measurement results will be presented.

- Gaining access to the traction battery pack terminals in a non-destructive way
- Designing a mobile unit able to discharge the battery at a constant current
- Quantify the auxiliary consumption delivered from the traction battery during the capacity measurement
- Determining the internal resistance of the battery at different SOC to allow SOH estimations

3.2.1 Gaining access to the traction battery through DC fast charge connector

When measuring the battery capacity based on a full discharge, the result is independent of drivetrain, on-board chargers, etc. imposes the requirement of a direct link between the traction battery and an external discharging device. The DC fast charge connector found on a number of modern EVs offers such a link.

However, for the CHAdeMO connector, found on a number of vehicles used in the on-road tests as part of the Green eMotion project, the right sequence of engaging analogue control lines and CAN bus communication (through the CAN bus embedded in the CHAdeMO connector), is mandatory to establish connection between the traction battery and the external CHAdeMO.

Furthermore, when the connection has been established, the CAN bus communication must be maintained and the CHAdeMO charger must deliver the current requested by the vehicle, to maintain the connection. While this procedure is well described for vehicle charging, the protocol did not appear to support vehicle discharge at the time this was investigated, as only a positive charging current parameter was allowed to be send from the CHAdeMO unit to the vehicle.

In order to demonstrate how discharging through the DC fast charge connector can be performed, once the CAN communication challenge has been addressed, a DC fast charge connector without CHAdeMO restrictions has been retrofitted to an electric Fiat Fiorino.

3.2.2 Designing a mobile load bank

A constant current discharge can be obtained in a number of ways. The energy absorbed from the traction battery may either be injected to the electrical grid through a grid tied inverter of which the output power is controlled based on the input current delivered from the battery, or the energy may be dissipated as heat.

As a grid tied inverter requires a grid allowing injection of power in the range of 5-15 kW, this solution will dramatically limit the mobility and flexibility. On the other hand, a DC load bank dissipating the energy as heat does not require a grid connection as the limited amount of power consumed by the control unit and cooling fan can be supplied from either a DC/AC inverter or generator installed in the service vehicle carrying the load bank. Please see section 3.3 and Figure 3.2.1.

Figure 3.2.1: The mobile load bank in action on parking lot in Aarhus, Denmark

3.2.3 Quantifying the auxiliary consumption during capacity measurements

During a constant current discharge, the battery voltage as well as the current entering the load bank are monitored using high precision sensors embedded as part of the mobile load bank. This allows accurate measurement of the accumulated energy (kilowatt-hours) absorbed by the load bank.

However, depending on the type of EV there may be auxiliary equipment consuming power which must be taken into account to obtain a reliable capacity measurement. Preferably all auxiliary equipment is disabled to achieve a negligible measurement error. In case this is impractical, or in case the power consumers leading to auxiliary consumption cannot be located, the total battery current (including auxiliary consumption) must be monitored during discharge either through the vehicle CAN bus or through current sensor(s) mounted on the vehicle under test.

3.2.4 Automated internal resistance measurement

The internal resistance of the battery is expected to increase over the lifetime of the battery. And will furthermore influence on the power handling of the battery, as the voltage sag under load is proportional to the internal resistance. Therefore, it is relevant to implement an automated pulse discharge load profile, which allows determination of the internal resistance. The internal resistance will depend on battery temperature and SOC. The measurement must therefore either be carried out under similar temperature conditions each time, or the temperature differences must be compensated for.

Furthermore, the SOC must be known at the start of the test to allow the automated load profile to perform measurements at predefined SOC levels. Please see Figure 3.2.2.

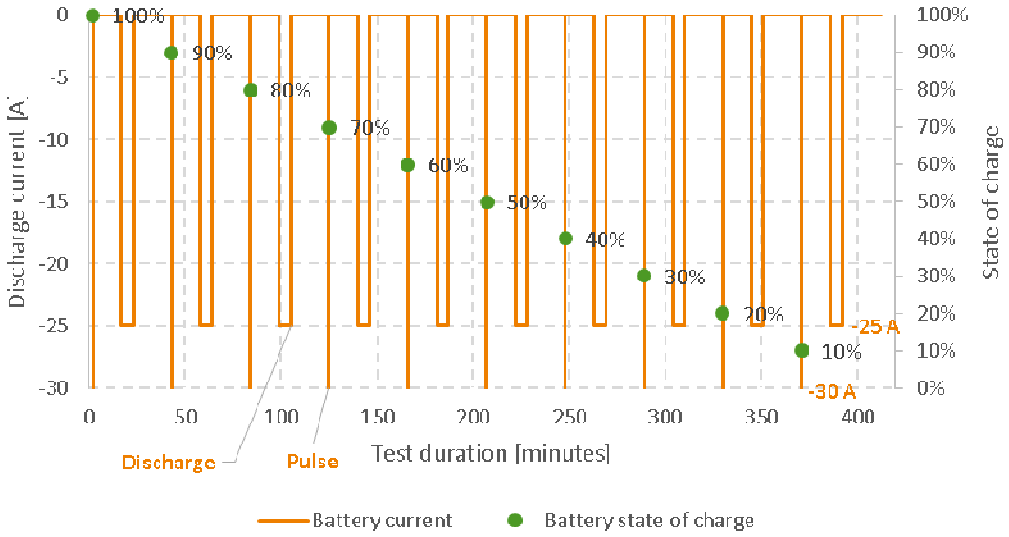

Figure 3.2.2: Visualizing the load sequence

Prior to the test, the battery is charged to 100% SOC. The automated test will perform an internal resistance measurement at 100, 90, 80, 70, 60, 50, 40, 30, 20, 10% SOC, by initiate a measurements of the OCV at no load (U1 at I1=0A), followed by a high resolution voltage measurement performed, while a 30A current pulse with a duration of 1 second is applied. In the end of the pulse another measurement is performed (U2 and I2). Please see Figure 3.2.3.

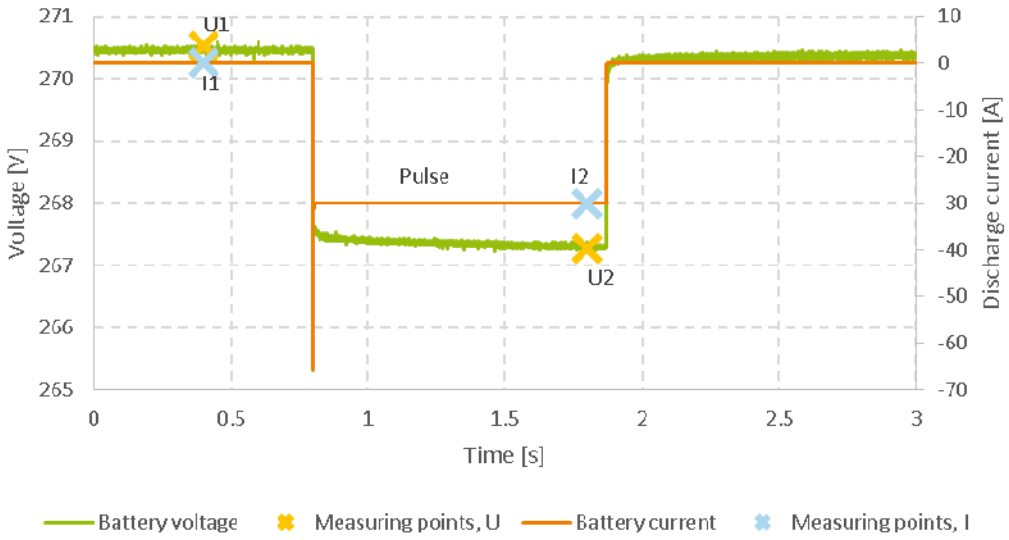

Figure 3.2.3: Example of measured pulse used to determine battery internal resistance, at 50% SOC

After the pulse has been applied, the battery is allowed a 20 minute resting time, after which the OCV is measured again (U3 and I3). Subsequently the battery is discharged at C/3 to 90% SOC and allowed a 15 minute resting time, before the pulse sequence is repeated. Please see Figure 3.2.4. This procedure is repeated in steps of 10% SOC until a SOC of 10% has been reached.

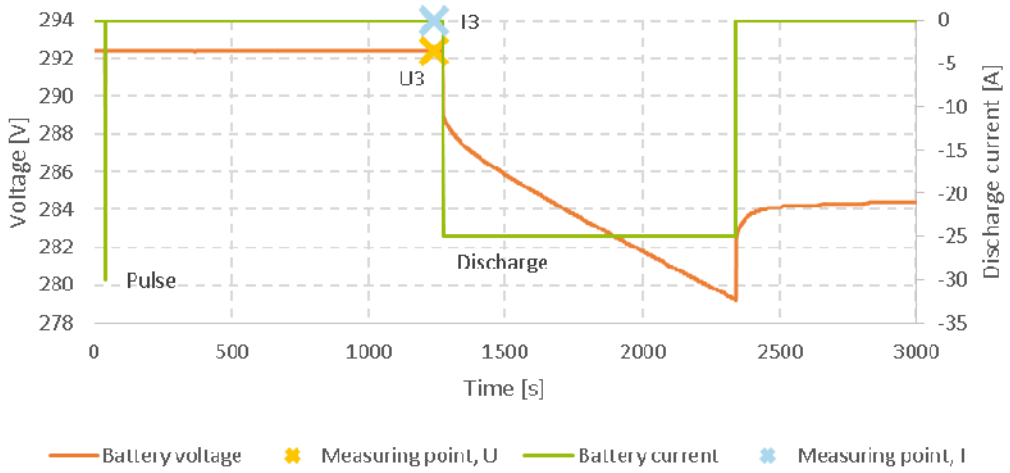

Figure 3.2.4: Example of measured battery discharge period, 100% to 90% SOC at 25A

The battery voltage in Figure 3.2.4 has a steep slope, because the battery is at high level SOC (100% going to 90%). To the far right hand side, a determination pulse for the battery internal resistance is shown.

3.3 Hardware and software implementation

Following chapter describes the physical implementation of equipment needed to perform capacity test through DC connector.

3.3.1 Implementation of load bank and associated data acquisition equipment

The load bank unit integrates the equipment mentioned below in a mobile rack, which can be used while mounted in the battery service vehicle, or as a free standing device.

- TDI WCL488 400-1000-1200, 12 kW water-cooled DC load bank
- EA-PS 8080-340, 0-80V and 0-340A DC power supply
- Radiator and fan allowing heat dissipation to ambient air
- Light weight circulation pump
- National Instruments data acquisition unit for data logging

The implemented system allows discharge of EV battery packs with a maximum voltage of up to 400V. The constant discharge current can be adjusted from 0A to 12kW (maximum battery voltage).

Furthermore, the integrated power supply allows charging of non-road utility EVs and has been embedded to allow faster charging, as the on-board charger on such vehicles often is dimensioned for over-night charging (small-current charging).

Figure 3.3.1: Mobile load bank unit in the battery service vehicle

3.3.2 Implementation of DC fast charge connector

To allow a safe access to the battery pack a touch safe DC charging/discharging connector has been retrofitted. The connector is located below the AC connector to create a connector similar to the J1772 DC combo connector and is electrically connected, through a fast acting fuse, to the positive and negative bus bar in the motor inverter enclosure.

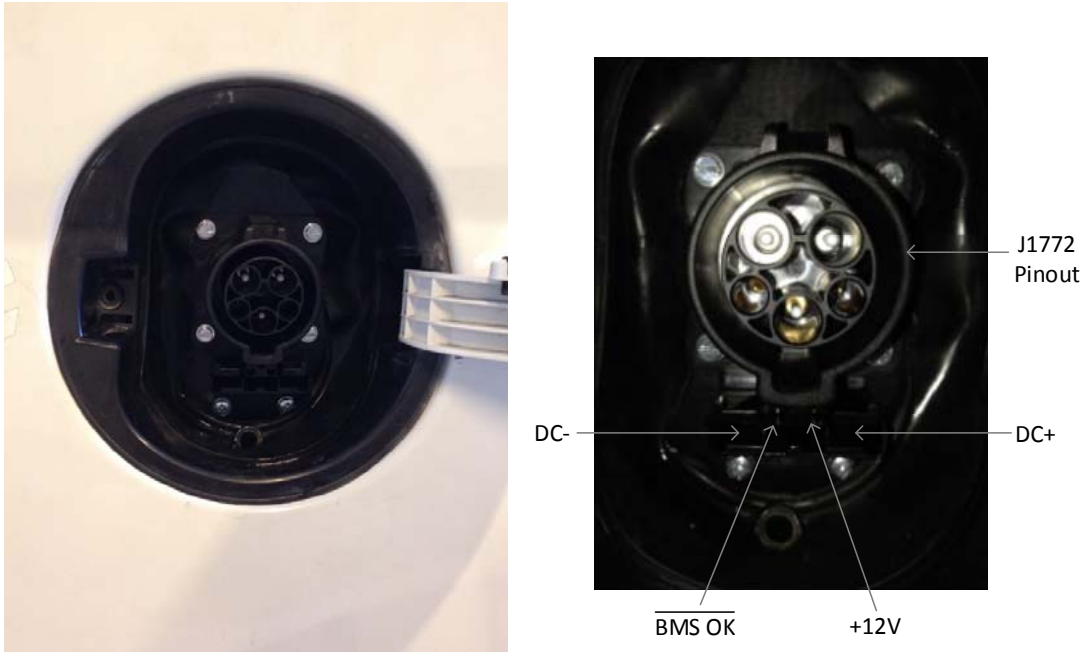

Figure 3.3.2: Retrofitted J1772, DC connector and pin-out

The electrical connection is established on the secondary side of the battery main contactor relay, meaning that the current flow in the retrofitted DC connector can be interrupted by the vehicles BMS, in case of an out of the safe operation area situation.

In addition to the direct protection of the wires carrying the charge/discharge current, a signal from the BMS has been embedded in the DC connector, which ensures redundant protection of the battery, as this signal will disable the load bank if a failure is detected by the BMS.

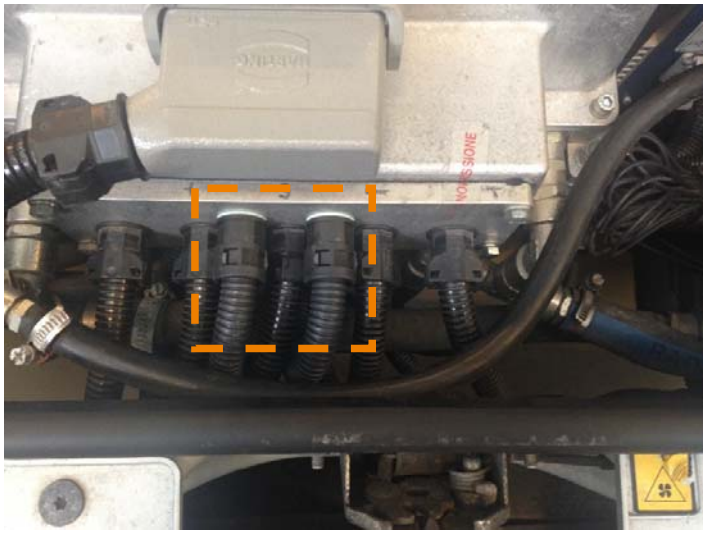

Figure 3.3.3: Upper cable conduits are retrofitted for DC connector

3.3.3 Improvements to increase EV usability

As easy access to charging facilities is a keyword for EV users, a number of improvements have been implemented on the Fiat Fiorino to increase the flexibility.

- The AC charging connector has been upgraded from CEE to J1772 to allow use of the charging facilities in public places.
- The charging power has been reduced to a maximum of 2300W to allow charging from ordinary 230V, 10A domestic outlet (through J1772 cable adaptor), without the risk of blown fuses.

3.3.4 Pulse discharging during driving

Similar to the automated measurements in section 3.2.4, a test can be performed manually in the field an EV from which the battery internal resistance can be determined. Accelerating and recuperating is done repeatedly to mimic a step response test, which is shown in Figure 3.3.4.

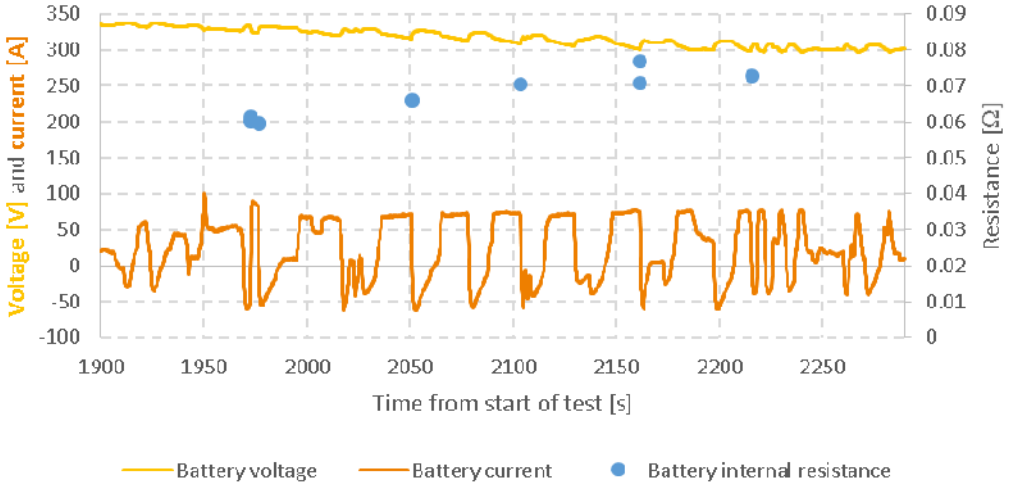

Figure 3.3.4: Non-intrusive field measurements of step response with Renault Fluence ZE

In Figure 3.3.4 the internal resistance is determined by processing the recorded data and detecting the step edges in the current. At these edges the steady state voltage values and the corresponding current values are used to calculate the internal resistance like described in section 3.2.4.

3.3.5 C/3 discharging

When using the EV as a test rig it is complicated to keep the discharge power constant. Therefore, the standard C/3 discharge was replaced with the Standardized On-Road Driving Scheme (SORDS).

The measured mean battery power during SORDS driving with the EVs used in the on-road tests is shown in Table 3.2 expressed in C-rate. The C-rates are a bit above the C/3, but they are all below 1C and relatively constant per vehicle respectively. The C-rates vary naturally with the vehicles, because of the different battery energy capacities,

	Nominal HV battery capacity	**Mean HV battery discharge rate**
Nissan Leaf	24 kWh	0.62 C
Renault Fluence ZE	22 kWh	0.76 C
Mitsubishi i-MiEV	16 kWh	0.63 C
Tesla Model S	85 kWh	0.20 C
Fiat Fiorino Micro-Vett	31 kWh	0.54 C
Fiat Fiorino Enerblu	20 kWh	0.84 C

Table 3.2: Mean discharge rate during SORDS driving

The charge rates shown in Table 3.3 are almost perfectly constant. These are common slow charge rates (small-current charging), which are near C/10.

	Nominal HV-battery capacity	Battery charge rate	AC power
Nissan Leaf	24 kWh	0.10 C	2.30 kW
Renault Fluence ZE	22 kWh	0.10 C	2.30 kW
Mitsubishi i-MiEV	16 kWh	0.14 C	2.30 kW
Tesla Model S	85 kWh	0.08 C	6.40 kW
Fiat Fiorino Micro-Vett	31 kWh	0.07 C	2.30 kW
Fiat Fiorino Enerblu	20 kWh	0.12 C	2.30 kW

Table 3.3: Charge rate during vehicle standard slow charge

Most lithium-ion batteries have slightly asymmetric charge/discharge characteristics specified by the manufacturer, but the maximum rates are typically several Cs both in and out for a short period of time, including cell temperature monitoring and of course not exceeding the maximum allowed cell temperature.

3.3.6 Capacity vs. temperature

To draw a conclusion on how the ambient temperature influences the battery capacity, one needs to perform capacity measurements in acclimatized environments.

Such measurements have been performed by Waterloo University and TÜV NORD Mobilität. Additional points have been observed by the Green eMotion team during the work, which support the tendency of Waterloo University's results. These are shown in Figure 3.3.5.

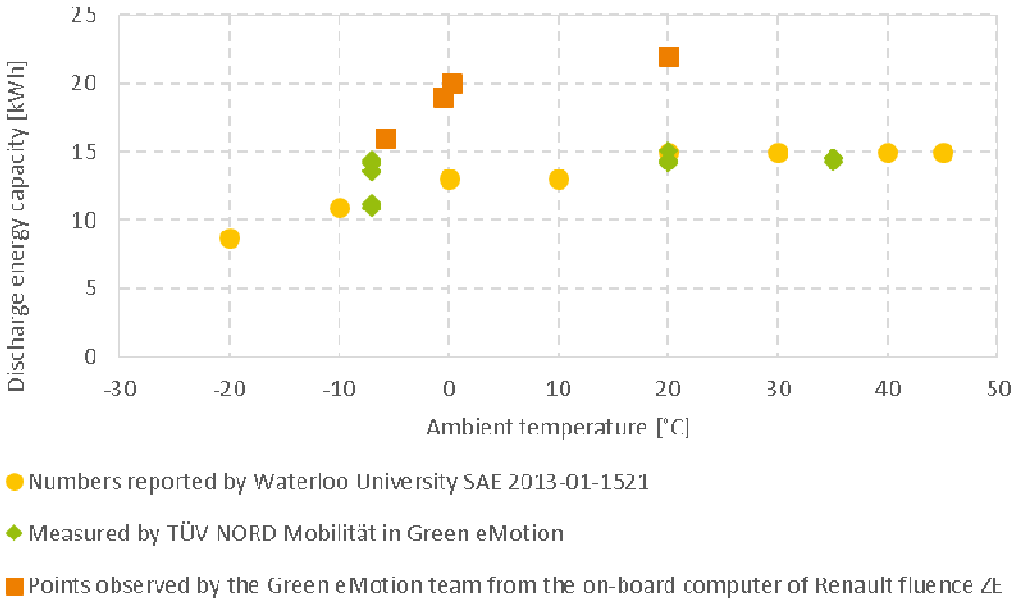

Figure 3.3.5: Energy capacity versus ambient temperature

The report on the outcome of the RekkEVidde Project[1] was read with great interest. In the report, the energy uptake was measured with a Citroën C-Zero tested at a dynamometer in a climate chamber. Even though no actual capacity measurements were shown in the report, it is mentioned that the personnel did not see any significant change, with respect to the ambient temperature, in the amount of energy charged to the EV battery from the grid.

3.3.7 Battery efficiency

By adding energy from the grid to any battery, this energy is stored. Discharging the energy from the same battery it is not possible to regain the same amount of energy. A part of it is lost in the charger, but also in the battery itself. This relationship between the energy discharged with the EV on the road and the originally charged energy from the grid is hereby defined as the so-called grid-to-road efficiency.

The normal level of charging efficiency would be around 85% for charger, including a transformer, and the efficiency of a Lithium-Ion battery is around 90-95% at dynamic load. In total an efficiency around 76-81%.

Some of the examples of battery efficiencies shown in Figure 3.3.6 are very low (approximately 56-61%). This may be due to a slightly lower power factor. The Fiat Fiorino Enerblu was discharged through the mobile load bank at lower constant load (C/3). This would explain its higher efficiency.

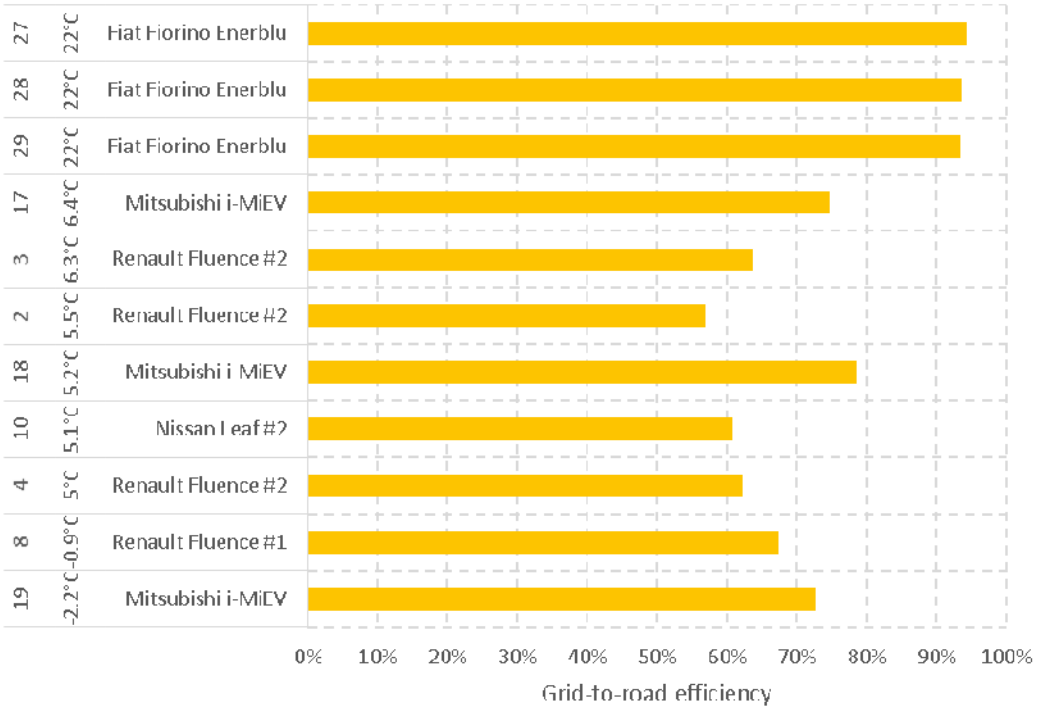

Figure 3.3.6: Grid-to-road efficiencies for the EVs used in the on-road tests

[1] Haakana A, Laurikko J, Granström R, Hagman R. "Assessing range and performance of electric vehicles in Nordic driving conditions –End of Project Report". Project RekkEVidde. December 2013.

For information about powertrain efficiencies please see D6.2.

3.4 Battery modelling

Types of battery models available today include electrochemical models, neural network models, thermally coupled models, etc. For this project we chose to model via an equivalent electrical circuit. This model serves as an indicator of the battery state of health, while trying to replace EIS measurements on EVs with unknown cell chemistry and when not having access to the battery terminals.

When having an accurate model of a battery, one can simulate the battery response to a certain stimuli without being forced to test the battery in the field. However, a simplified battery model can still qualify to a narrower scope of application. The possibility of an electrochemical model has been eliminated, because crucial information about the cell chemistry was not available.

The battery model is a physical discharge model based on the electrical elements inside a real EV battery during discharge. The model includes everything in the line of power; bus bars, fuses, contactors etc. The model does not include the known influence from the temperature, but the ambient temperature has been logged during the tests and is compared whenever possible.

The equivalent circuit of the battery became the 2nd order Randle circuit, including a voltage source representing the battery OCV, as inspired by literature[2], because we found that it corresponded extremely well with our measured data. All impedances in the line of power are included in these five elements.

3.4.1 Equivalent circuit model

As mentioned earlier, the 2nd order Randle circuit, as shown in Figure 3.4.1, has been selected as equivalent electrical circuit to model the internal impedance of lithium-ion batteries in the Green eMotion Project.

[2] Hu X. and Stanton S, ”A Complete Li-Ion Battery Simulation Model”, SAE Technical Paper 2014-1-1842, 2014, doi:10.4271/2014-01-1842.

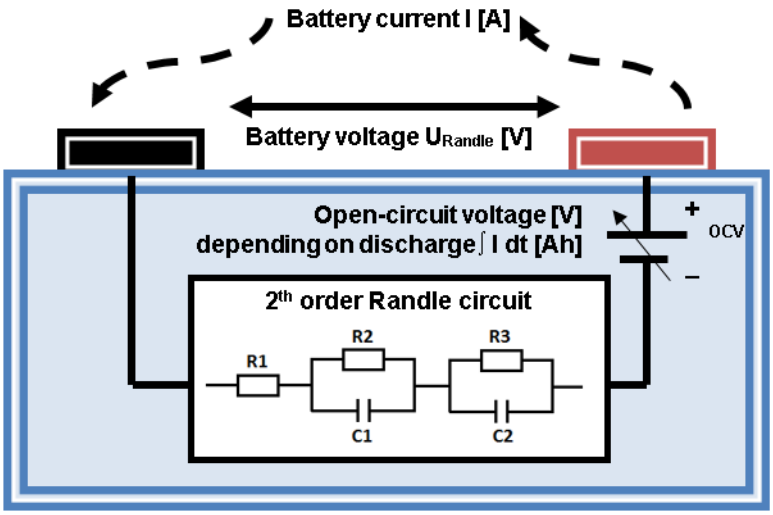

Figure 3.4.1: 2nd order Randle circuit model

The internal impedance of the battery is then modelled by the 2nd order Randle circuit, whereto the OCV is a vital part to produce accurate Randle coefficients, which are the resistance and capacitance values of the circuit.

Starting with the OCV:

The ideal battery element serves as a SOC-dependent voltage generator. The function of the voltage generator is based on the formula for calculation of volume of rotational solid around the x-axis of a system of coordinates. The volume of the rotational solid is the SOC in Ampere-hours, a charge container or "the bohemian floor vase", which can be calculated from the CAN battery current. The height of the charge container on the x-axis is the OCV with the initial condition of the battery voltage at no load at the starting point of the discharge test. Please see Figure 3.4.2.

The formula for the "charge container" is expressed as below, where *a* and *b* are the minimum and maximum OCV respectively:

$$SOC(OCV) = \int_{a}^{b} \pi \cdot f(OCV)^2 dOCV \qquad (1)$$

Rewriting (1), the change in OCV can be expressed as in (2) below:

$$dOCV = \frac{dSOC}{f(OCV)^2 \cdot \pi} \qquad (2)$$

Solving (2), one needs to guess the function of OCV, which is the radius of the "charge container". A qualifying function was found to as expressed in (3), where α, σ, μ and *K* are all constants:

$$f(OCV) = \alpha \frac{1}{\sigma\sqrt{2\pi}} \cdot e^{-(OCV-\mu)^2/(2\sigma^2)} + K \qquad (3)$$

When inserting (3) in (2), the change in OCV can easy be calculated from the change in SOC during discharge.

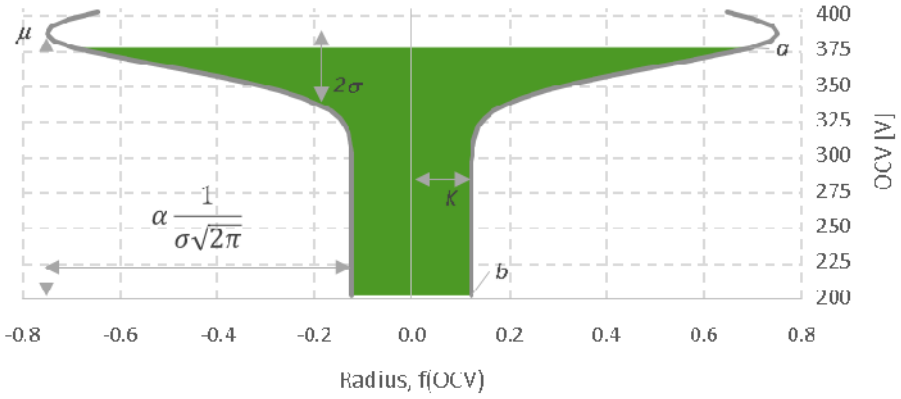

Figure 3.4.2: Illustration of the OCV volume model, "the bohemian floor vase"

Then the Randle coefficients:

The 2nd order Randle circuit consist of three resistances (R_1, R_2 and R_3), where the sum of resistances reflects the DC resistance of the battery. R_2 and R_3 sits in pairs with two capacitances respectively as shown in Figure 3.4.1.

The coefficient values can be found by applying the regular formulas for RC-circuits, including Ohm's law and Kirchhoff's laws.

Finding the current through resistor R1:

$$I_{R1} = I_{Batt} \tag{4}$$

Finding the current through resistor R2:

Current through capacitor C1:

$$I_{C1} = C1 * R2 * \frac{dI_{R2}}{dt} \quad (5)$$

Inserting (5) in Kirchhoff's law gives the expression in (6):

$$I_{R1} = I_{R2} + C1 * R2 * \frac{\Delta I_{R2}}{\Delta t} \quad (6)$$

Rewriting (6):

$$I_{R1} - I_{R2} = C1 * R2 * \frac{\Delta I_{R2}}{\Delta t} \quad (7)$$

Rewriting (7):

$$(I_{R1} - I_{R2}) * \Delta t = C1 * R2 * \Delta I_{R2} \quad (8)$$

Which can then be reduced to:

$$\Delta I_{R2} = \left(\frac{I_{R1} - I_{R2}}{C1 * R2}\right) * \Delta t \quad (9)$$

Finding the current through resistor R3:

Current through capacitor C2:

$$I_{C2} = C2 * R3 * \frac{dI_{R3}}{dt} \quad (10)$$

Inserting (10) in Kirchhoff's law gives the expression in (11):

$$I_{R1} = I_{R3} + C2 * R3 * \frac{\Delta I_{R3}}{\Delta t} \quad (11)$$

Rewriting (11):

$$I_{R1} - I_{R3} = C2 * R3 * \frac{\Delta I_{R3}}{\Delta t} \quad (12)$$

Rewriting (12):

$$(I_{R1} - I_{R3}) * \Delta t = C2 * R3 * \Delta I_{R3} \quad (13)$$

Which can then be reduced to:

$$\Delta I_{R3} = \left(\frac{I_{R1} - I_{R3}}{C2 * R3}\right) * \Delta t \quad (14)$$

Finding the so-called Randle-voltage:

The final voltage of the whole circuit loop can be expressed as (15):

$$U_{Randle}(t) = U_{OC}(t) - R_1 * I_{R1}(t) - R_2 * I_{R2}(t) - R_3 * I_{R3}(t) \quad (15)$$

Inserting the information from (4), (9), (14) and considering the sampling time gives the resulting equation shown in (16), where f_s is the sampling frequency at 10 kHz:

$$U_{Randle}(t) = U_{OC}(t) - R_1 * I_1(t) - R_2\left(\frac{I_{R1}(t) + f_s * I_{R2}(t-1) * C_1 * R_2}{1 + f_s * C_1 * R_2}\right) - R_3\left(\frac{I_{R1}(t) + f_s * I_{R3}(t-1) * C_2 * R_3}{1 + f_s * C_2 * R_3}\right) \quad (16)$$

The initial condition of U_{Randle} is the battery voltage at no load (OCV) at the starting point of the discharge test. The currents in R_2 and R_3 are initially 0 A. The spread inductance in the circuit is not included.

All together giving the 2nd order Randle battery model:

The OCV and the Randle coefficients is calculated from the CAN bus battery current and curve-fitted to the CAN bus battery voltage. From here the voltage response from an EV battery, in its current SOH, can be simulated with only the battery current as input. Furthermore, the Randle coefficients of a battery can be followed throughout the lifecycle to reveal the progress of the degradation.

Unfortunately, the equation in (3) can only be fitted to power flow in one direction at a time, where the discharge test includes the most fluctuating load, hence the highest AC content of the data.

3.4.2 Full performance sheet

Based on the model coefficients, it is possible to create a full performance diagram for one battery. A full performance diagram shows the battery voltage versus the delivered charge or energy at several discharge rates, covering the spectrum in which the battery is specified by its manufacturer. In this case we do not have the manufacturer specifications, therefore we have used our own.

Since the discharge is controlled by voltage and the battery voltage depends on the load, the charge released by the BMS must also be load-dependent.

Additionally, the power loss depends on the load, because of the voltage drop across the internal resistance, hence the delivered energy. The charge delivered does not contain voltage information and therefore, if twice the current is drawn in half the time, the charge delivered is the same, but the power loss gets doubled, hence the energy delivered gets reduced. Please see the two expressions below:

$$E(I) = R \cdot I^2 \cdot t = I^2 \cdot t \quad (17)$$

$$E(2I) = R \cdot (2I)^2 \cdot \frac{t}{2} = 2 \cdot I^2 \cdot t \quad (18)$$

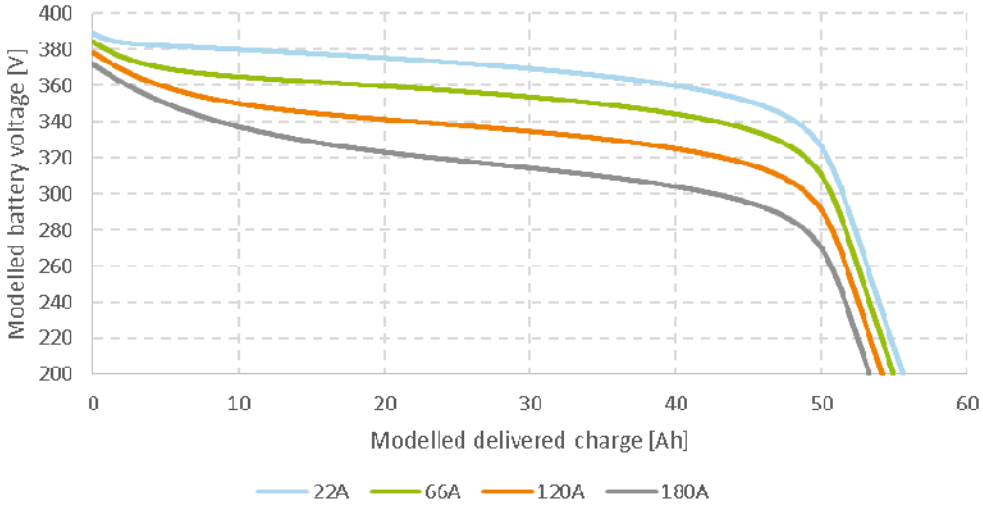

Figure 3.4.3: Discharge performance shown in charge (Ampere-hours), illustrated by Renault Fluence ZE battery (25-02-2014, 7.5°C).

It can be seen in Figure 3.4.3 that the delivered charge for the Renault Fluence ZE battery is almost independent of C-rate. Nevertheless, the delivered Ampere-hours vary much less than the kilowatt-hours shown in Figure 3.4.4, which is actually the area between the curve and the x-axis in Figure 3.4.3.

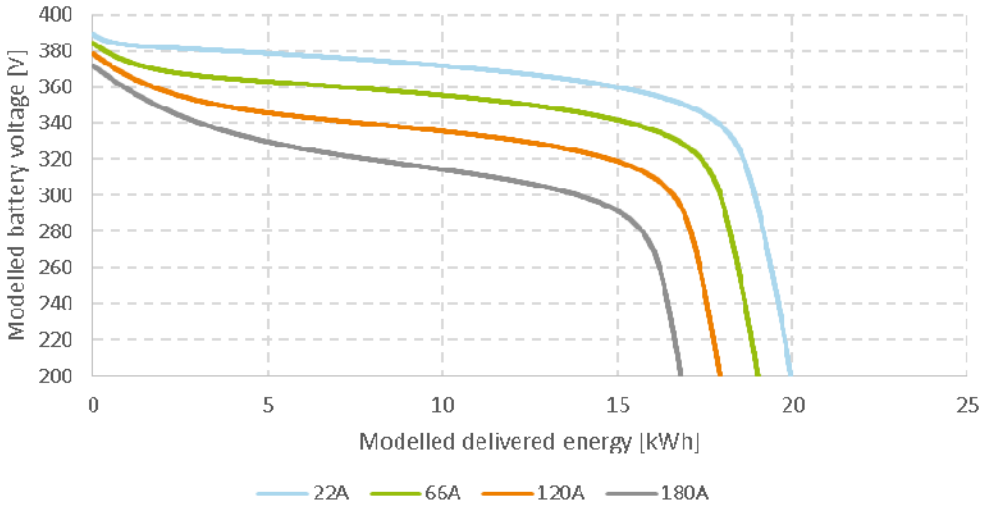

Figure 3.4.4: Discharge performance shown in energy, illustrated by Renault Fluence ZE battery (25-02-2014, 7.5°C).

All the data, from which the full performance diagrams in this section are based on, origin from the on-road tests performed in Karup 2013, where the weather conditions were similar.

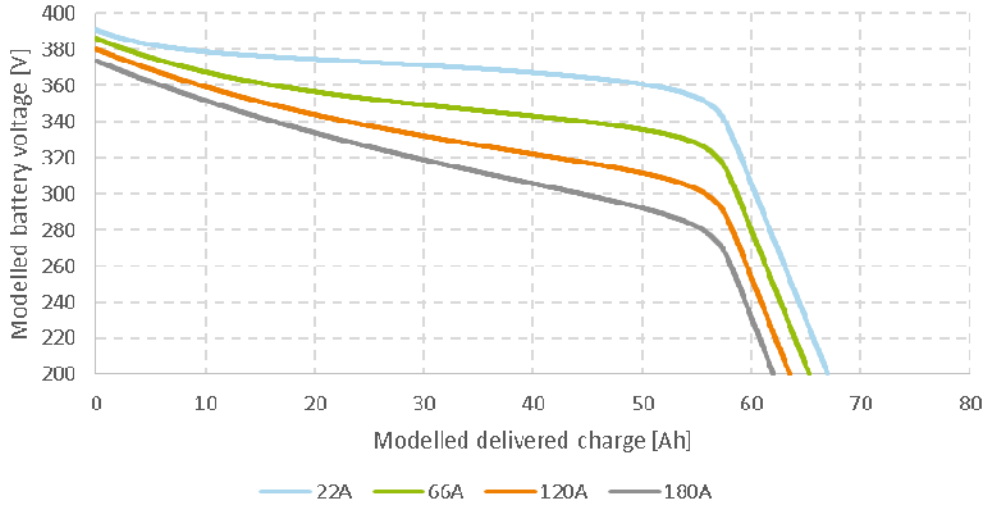

Figure 3.4.5: Discharge performance shown in charge (Ampere-hours), illustrated by Nissan Leaf battery (25-02-2014, 7.5°C).

The Nissan Leaf battery has slightly larger capacity than the Renault Fluence (approximately 4 kWh), but the battery performance appears to be almost the same.

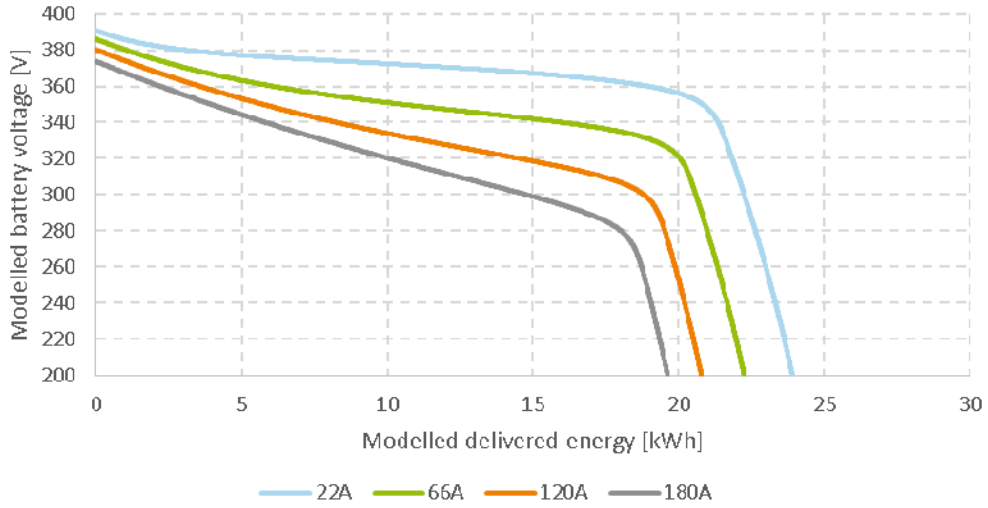

Figure 3.4.6: Discharge performance shown in energy, illustrated by Nissan Leaf battery (25-02-2014, 7.5°C).

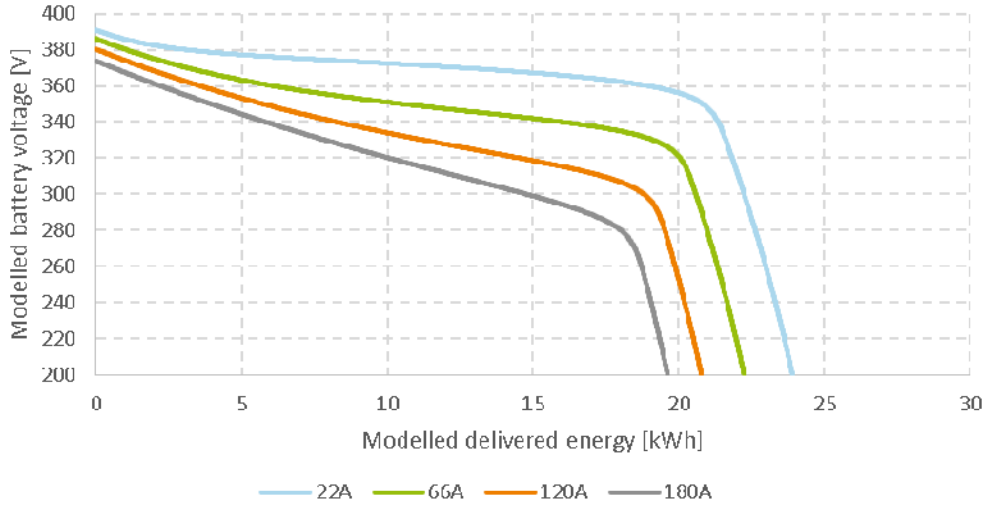

Figure 3.4.7: Reconstructed Nissan Leaf battery cell discharge characteristics

When comparing Figure 3.4.7 to Nissan's own data in Figure 3.4.8, one can see that the Randle model has relatively high precision. Please note that Figure 3.4.7 is based on battery pack data downscaled to cell voltage level, simply by dividing with the number of cells. This includes all the electric components in such EV system as used in the on-road tests.

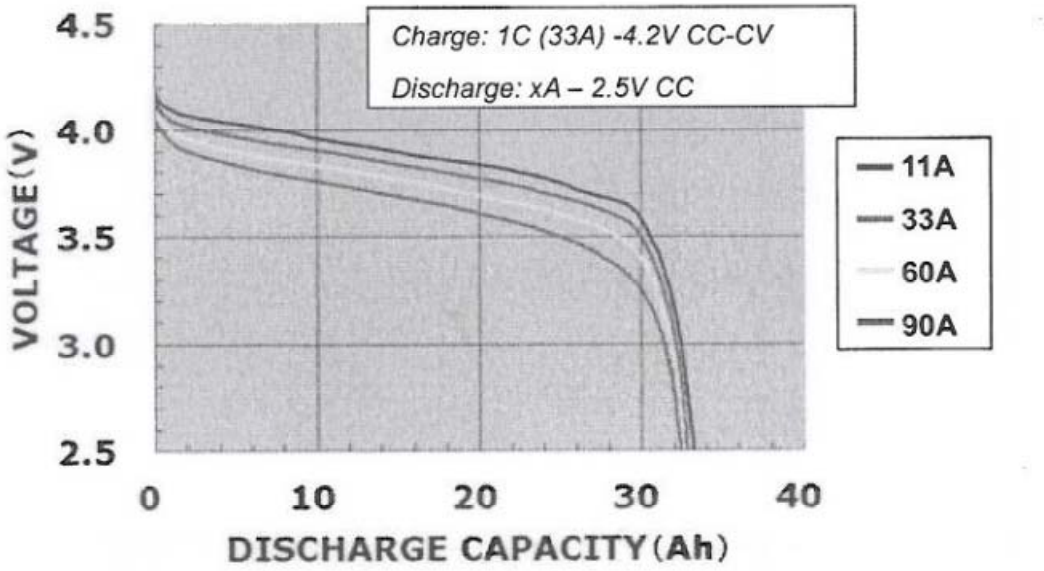

Figure 3.4.8: Nissan Leaf battery cell discharge characteristics[3]

[3] Ikezoe M. et al. "Developement of High Capacity Lithium-Ion Battery for NISSAN LEAF". 2012. SAE International.

3.4.3 Power losses in battery model

The power loss may be calculated as a combination of the resistive and capacitive parts of the 2nd order Randle circuit. Resistive elements do always involve direct real values as loss, whereas reactive elements like capacitive and inductive elements are only reactive losses. In the non-ideal world capacitors and inductors include real losses, because of the material used as conductor. Losses of ideal reactive elements are pure imaginary values.

In the case with the battery model, the 2nd order Randle circuit is a parasitic part of a non-ideal battery. Given the fact that all constructive materials have resistive properties, likewise reactive properties.

The conducting parts of the battery, the electrodes, yield primarily a direct power loss – dissipated into heat. Whereas the dielectric layers of the battery yield primarily a reactive loss. The electrodes and the dielectric materials are typically laid in sandwich formation, which can be stacked, rolled or combined. The described sandwich formation looks electrically like a plate capacitor and therefore there must be a dielectric loss, just like in a non-ideal capacitor.

The total circuit impedance is then the ESR plus the ESX, which are expressed in the form $R + jX$. In the Randle circuit, the ESR is included in the resistive element and the reactance is assumed purely capacitive.

The direct power loss in the real part is simply $P_R = R * {I_R}^2$.

The reactive loss is more complex depending on the material conductivity and permittivity. Even though a battery is DC, it reacts to changing DC like with AC. Therefore, a dissipation factor, also known as the loss tangent ($\tan\delta$), can be calculated due to the non-ideal capacitor as a ratio between the real power loss and the reactive power oscillation in the same capacitor. However, the ESR is not visible with this model, as the resistance is included in the other resistances, hence the reactive loss is omitted here.

$$Dissipation\ factor = \frac{\sigma}{\varepsilon * \omega} = \tan\delta$$

Where σ is the dielectric's bulk conductivity, ω is the angular frequency of the AC current (as usual), ε is the lossless permittivity of the dielectric and C is the lossless capacitance.

3.4.4 Nyquist plot

The 2nd order Randle model allows a Nyquist plot to be constructed, just as if a physical EIS measurement has taken place. However, the 2nd Randle model is based on a full discharge cycle, which means that it cannot yield a Nyquist curve for a specific SOC level.

Impedance (commonly designated with the capital letter Z) consist of two parts; a real part (the resistance, commonly designated with the letters Re) and a complex part (the reactance, commonly designated with the letters Im), which is time-dependent. The time-dependent part is also called the imaginary part, hence the imaginary part of the impedance is "Im(Z)". Similarly "Re(Z)" is short for the real part of the impedance.

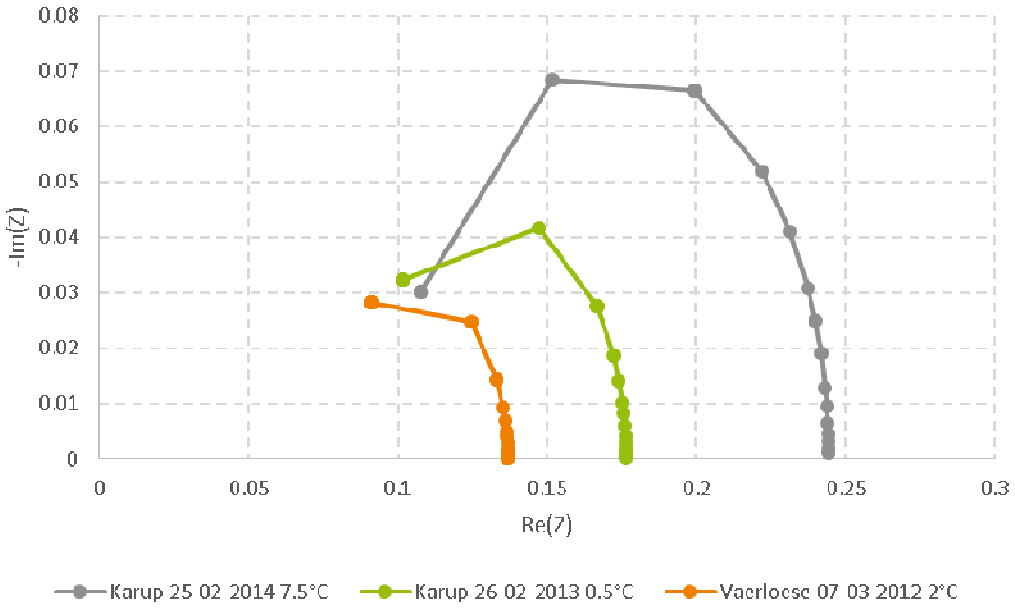

Figure 3.4.9: Nyquist plot of the Mitsubishi i-MiEV battery progressing over three years of time.

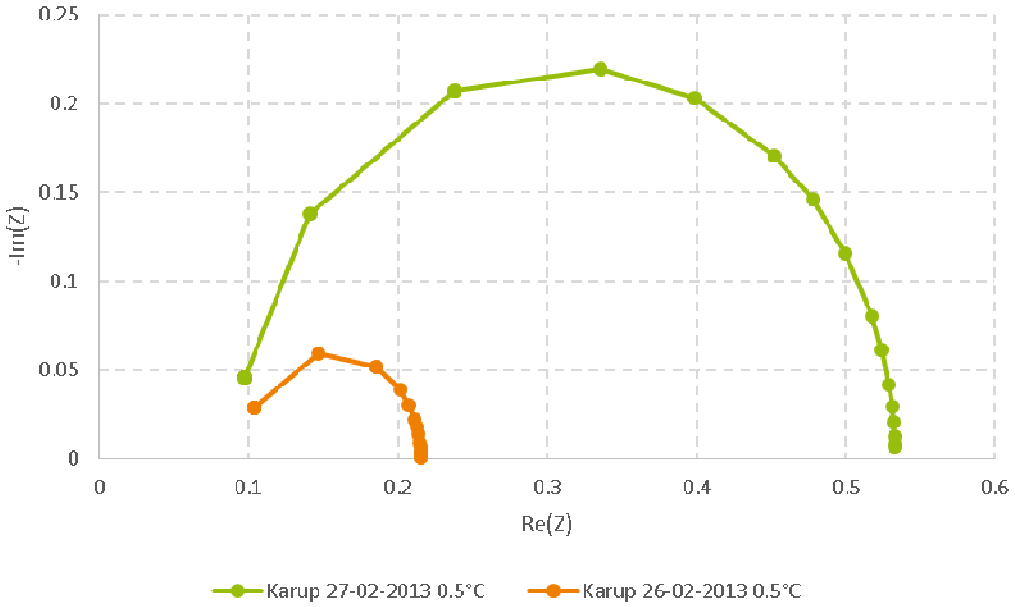

Figure 3.4.10: Nyquist plot of the Nissan Leaf battery short term progress. The vehicle was new (mileage: 50 km).

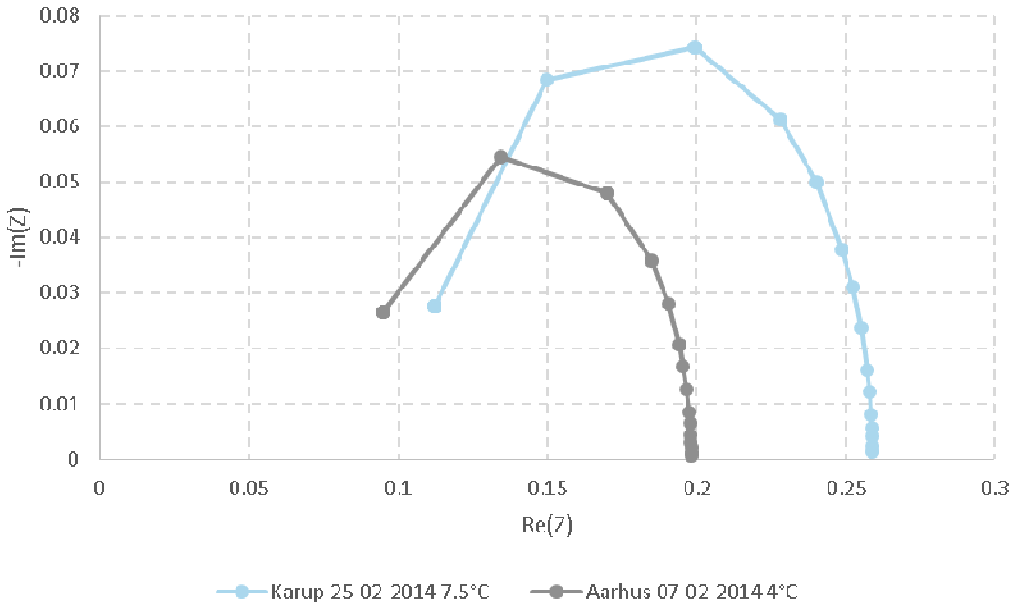

Figure 3.4.11: Nyquist plot of the Nissan Leaf battery short term progress. The 2014 Nissan Leaf was more experienced (mileage: 3,300 km) than the 2013 one.

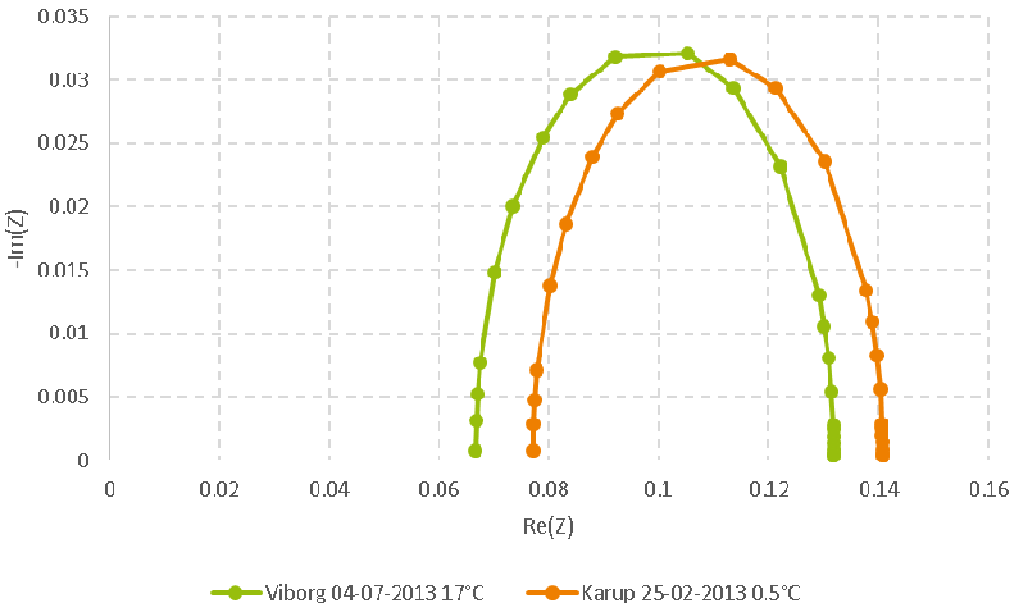

Figure 3.4.12: Nyquist plot of two different Renault Fluence ZE batteries.

3.4.5 EVPC pulse sequence simulation

Another way to characterize the battery SOH is by the EVPC pulse sequence[4], which is a series of values at different SOC showing the battery internal resistance and the power capability of the battery in the particular SOH.

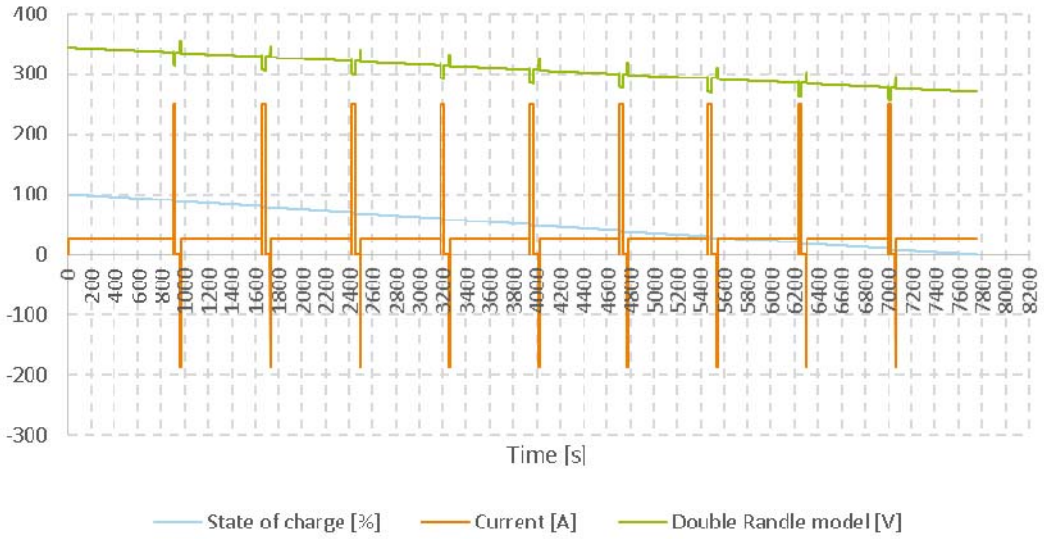

Figure 3.4.13: Input battery current and modelled voltage waveforms, illustrated by the Mitsubishi i-MiEV

The battery model was used to simulate the prescribed stimuli and the modelled battery voltage shown in Figure 3.4.13 were used to calculate the values in Figure 3.4.14 and Figure 3.4.15.

[4] Wishart J, Carlson R.B, Chambon P, Gray T. "The Electric Drive Advanced Battery (EDAB) Project: Developement and Utilization of an On-Road Energy Storage System Testbed". SAE International 2013-01-1533

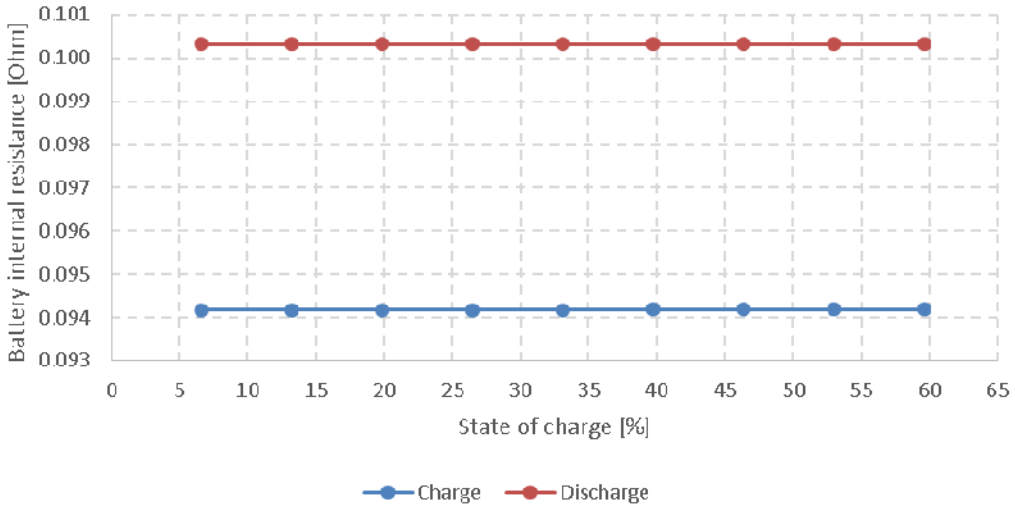

Figure 3.4.14: Battery internal resistances based on EVPC, illustrated by the Mitsubishi i-MiEV

The curves in Figure 3.4.14 show a rather constant internal resistance of the battery, which is not typical. In Figure 3.4.15 the battery power capability is decreasing with the SOC. This is the same tendency as the ISO 12405-2 simulation in section 3.4.6.

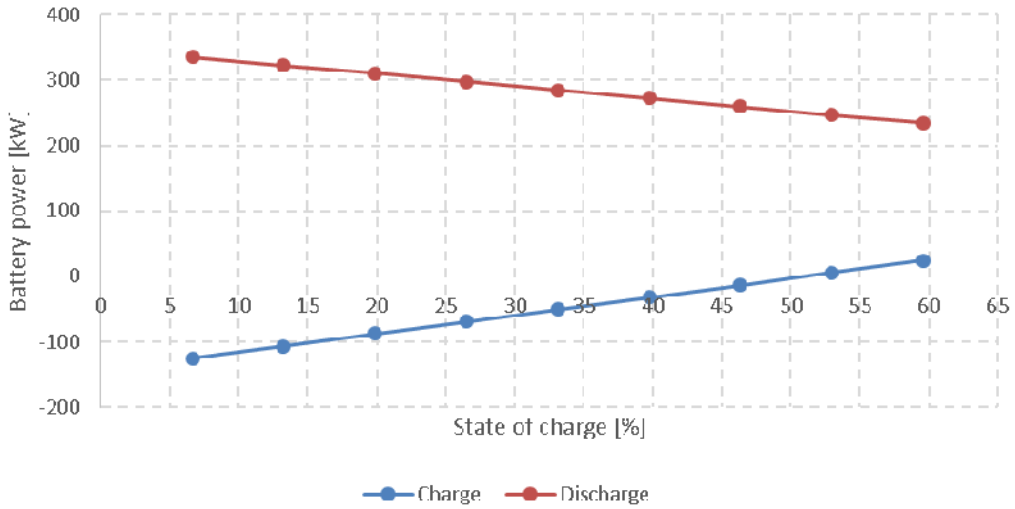

Figure 3.4.15: Battery power capability based on EVPC, illustrated by the Mitsubishi i-MiEV

3.4.6 ISO 12405-2 simulation

Again, the 2nd order Randle battery model was used to simulate the test. A virtual ISO12405-2 test was conducted with input current stimuli as shown in Figure 3.4.16 and the modelled result in Figure 3.4.17.

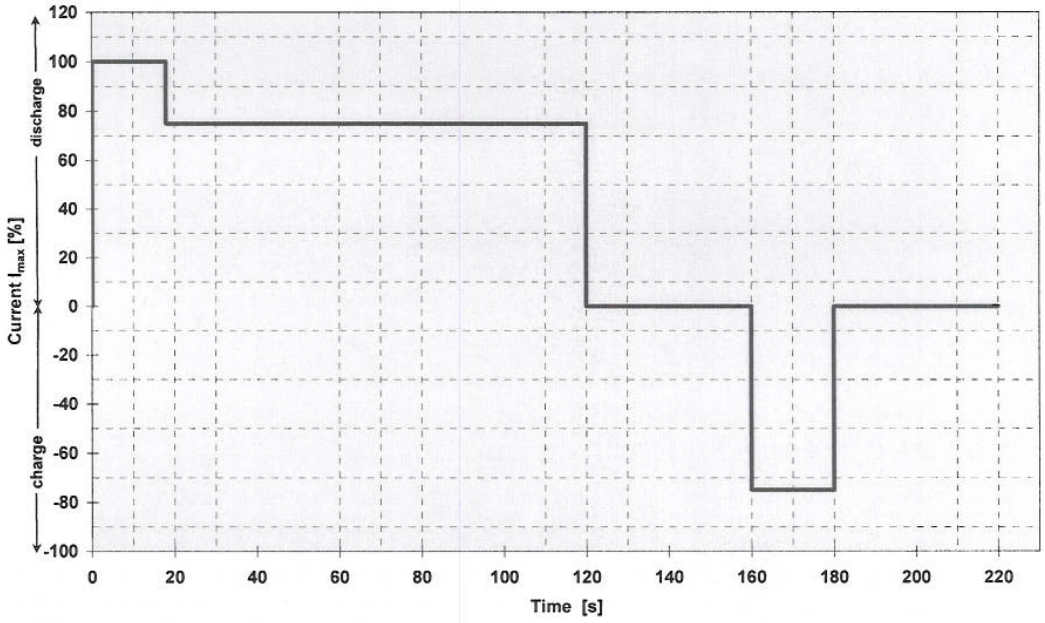

Figure 3.4.16: Pulse power characterization profile, current

Figure 3.4.17 does also show at which points the voltage values are used to calculate the sequence of resistance values and power values. These are 18 voltages values (U) with index numbered 0 to 17.

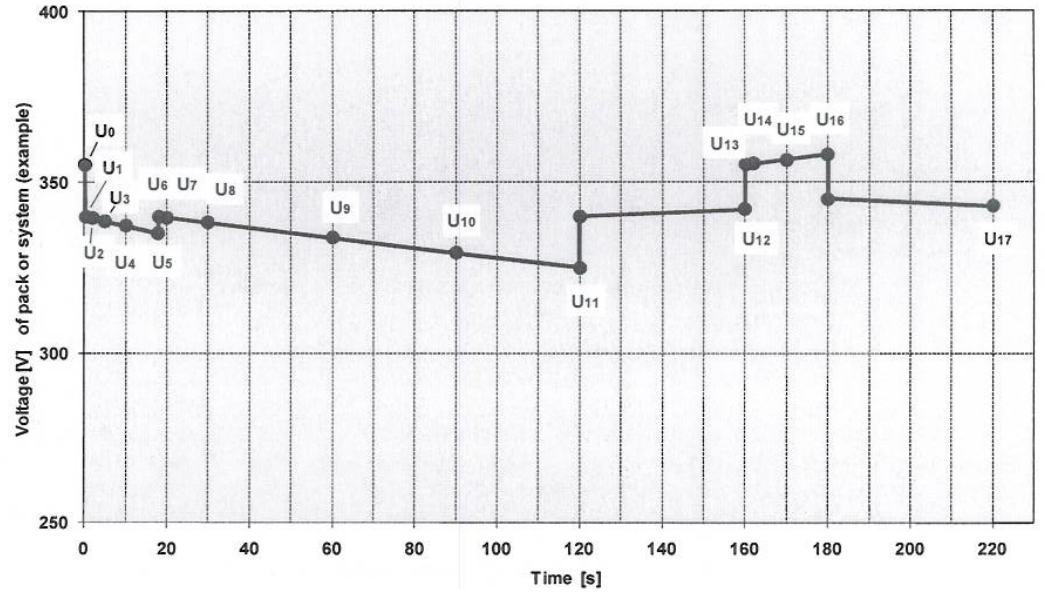

Figure 3.4.17: Pulse power characterization profile, example of voltage

From the modelled battery voltage response, the characteristic voltage values as shown in Figure 3.4.17 were extracted and the following resistance and power values were calculated. The time row represents the time prefix, e.g. the 0.1 column is the 0.1s discharge resistance in Table 3.4 and so forth. This description is also valid for Table 3.5 to Table 3.7.

Time [s] → Date of test ↓	0.1	2	5	10	18	18.1	20	30	60	90	120	Overall
Renault Fluence ZE												
2013-07-04	67	69	72	77	85	91	92	100	118	131	141	92
2013-02-25	78	80	84	89	97	104	106	114	132	146	155	103
2014-02-25	109	112	117	125	136	145	148	161	197	227	253	137
2014-02-26	97	99	102	106	113	117	119	127	149	170	188	114
Mitsubishi i-MiEV												
2012-03-07	78	83	89	100	115	128	131	145	178	201	217	133
2012-03-08	82	87	94	105	119	131	133	144	165	180	192	130
2013-02-26	84	90	100	113	129	145	147	157	178	191	201	138
2013-02-27	127	131	137	147	162	174	177	192	231	260	282	175
2014-02-25	102	107	114	126	143	157	161	178	218	245	262	156
Nissan Leaf												
2013-02-26	96	101	107	118	133	145	148	163	197	220	237	146
Vbox file 142 2014	93	99	109	124	148	167	172	199	271	332	383	151
2014-02-25	106	110	116	126	141	153	156	172	210	240	262	148

Table 3.4: Discharge resistance values in [mΩ] at 100% SOC according to ISO 12405-2

The corresponding resistance values for charging is shown in Table 3.5.

Time [s] → Date of test ↓	0.1	2	10	20	Overall
Renault Fluence ZE					
2013-07-04	67	70	81	94	64
2013-02-25	78	81	93	106	75
2014-02-25	109	114	131	151	96
2014-02-26	102	104	114	125	95
Mitsubishi i-MiEV					
2012-03-07	78	85	109	135	77
2012-03-08	82	88	109	130	100
2013-02-26	84	91	115	136	112
2013-02-27	127	133	156	183	115
2014-02-25	102	108	132	158	100
Nissan Leaf					
2013-02-26	96	102	125	149	93
Vbox file 142 2014	93	101	136	177	67
2014-02-25	106	111	132	157	95

Table 3.5: Charge resistance values in [mΩ] at 100% SOC according to ISO 12405-2
In Table 3.6 the discharge power capability is shown.

Time [s] → Date of test ↓	0.1	2	5	10	18	18.1	20	30	60	90	120
Renault Fluence ZE											
2013-07-04	95	94	94	94	93	71	71	71	70	69	69
2013-02-25	94	94	94	93	93	70	70	70	69	69	69
2014-02-25	91	91	90	90	89	68	68	68	66	65	64
2014-02-26	91	91	91	91	90	69	69	69	68	67	67
Mitsubishi i-MiEV											
2012-03-07	85	85	84	84	83	63	63	62	61	60	60
2012-03-08	83	83	83	82	81	62	62	61	61	60	60
2013-02-26	81	81	81	80	79	60	60	60	59	58	58
2013-02-27	81	80	80	79	78	60	60	60	58	57	56
2014-02-25	83	82	82	81	80	61	61	61	59	58	58
Nissan Leaf											
2013-02-26	91	91	90	90	89	68	68	67	66	65	64
Vbox file 142 2014	92	91	91	90	88	67	67	66	64	61	60
2014-02-25	92	92	92	91	90	69	69	68	67	66	65

Table 3.6: Discharge power values in [kW] at 100% SOC according to ISO 12405-2

The negative power values shown in Table 3.7 denote that the power is flowing into the battery, hence the load current is negative. This is the charge power capability.

Time [s] → Date of test ↓	0.1	2	10	20	OCV
Renault Fluence ZE					
2013-07-04	-69	-75	-75	-75	392
2013-02-25	-69	-75	-75	-76	391
2014-02-25	-64	-73	-73	-74	380
2014-02-26	-67	-74	-74	-75	382
Mitsubishi i-MiEV					
2012-03-07	-60	-67	-67	-68	355
2012-03-08	-60	-67	-67	-68	348
2013-02-26	-58	-66	-66	-67	340
2013-02-27	-56	-67	-67	-68	346
2014-02-25	-58	-67	-67	-68	347
Nissan Leaf					
2013-02-26	-64	-73	-73	-74	381
Vbox file 142 2014	-60	-68	-68	-70	367
2014-02-25	-65	-74	-74	-75	385

Table 3.7: Charge power values in [kW] and OCV in [V] at 100% SOC according to ISO 12405-2

3.4.7 Randle coefficients vs. age of battery

With age, the Randle coefficients seem to be changing.

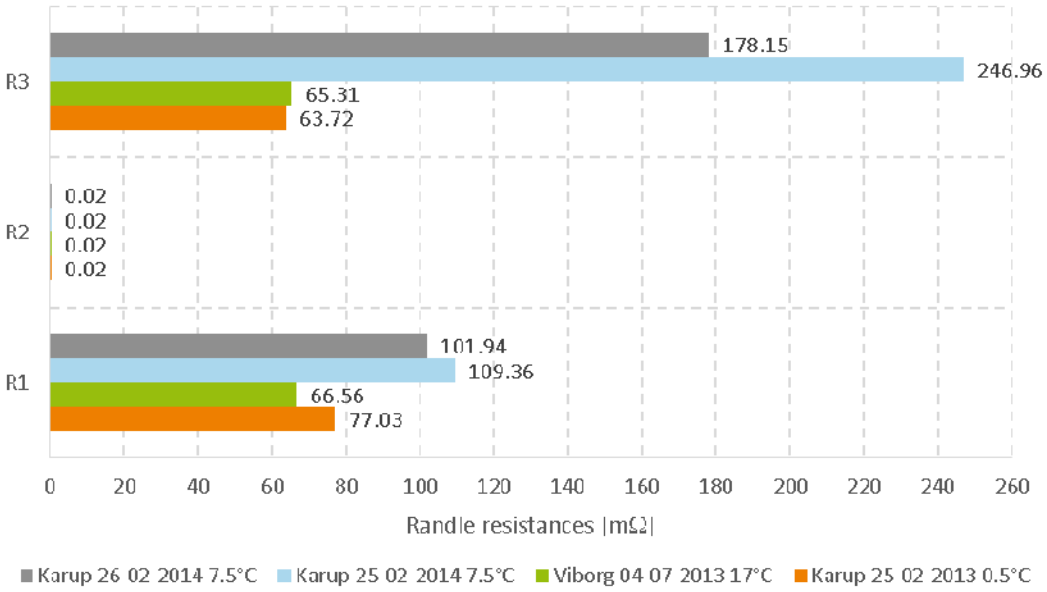

Figure 3.4.18: Randle resistances for the Renault Fluence batteries[5] used in the on-road tests.

Due to the fact that the battery swapping was still in operation in 2013, the possibility that the Renault Fluence ZE swapped its battery in between the test cannot be eliminated.

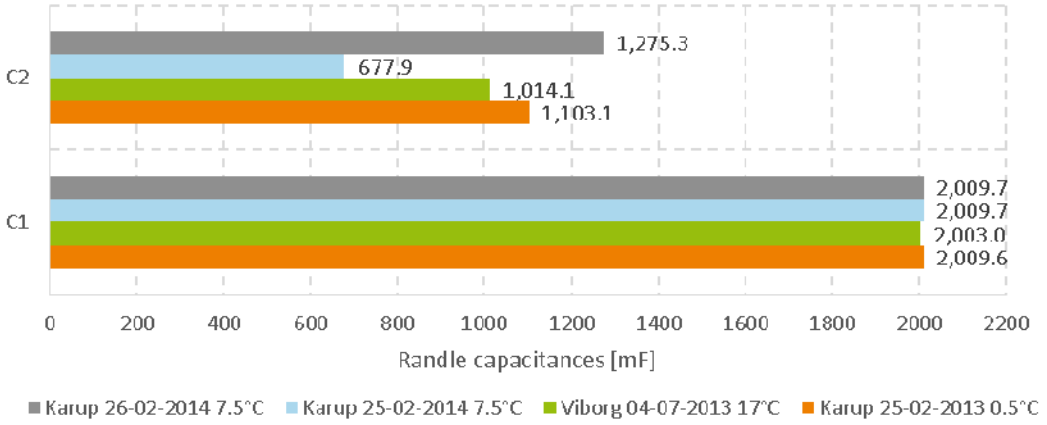

Figure 3.4.19: Randle capacitances for the Renault Fluence batteries5 used in the on-road tests.

[5] Note that different Renault Fluence ZE vehicles and batteries were used in the on-road tests.

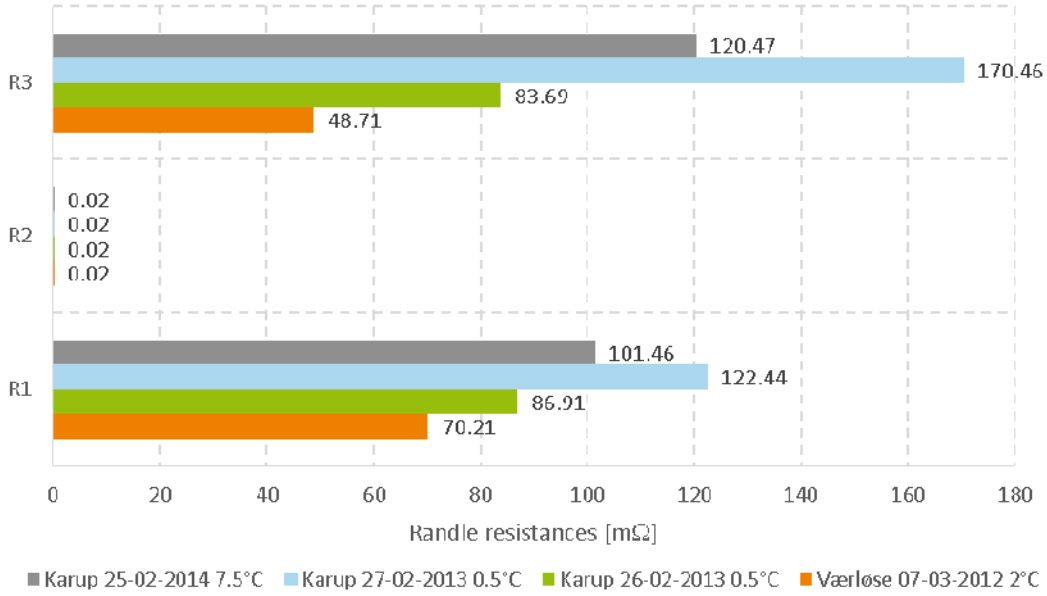

Figure 3.4.20: Randle resistances for the Mitsubishi i-MiEV batteries used in the on-road tests.

Concerning the Randle coefficients from the Mitsubishi i-MiEV, shown in Figure 3.4.20 and Figure 3.4.21, the good measured data did not include full discharge cycles. Therefore, these coefficients are less accurate than expected. Unfortunately, the Mitsubishi i-MiEV was the only exact same EV used all three times in the on-road tests.

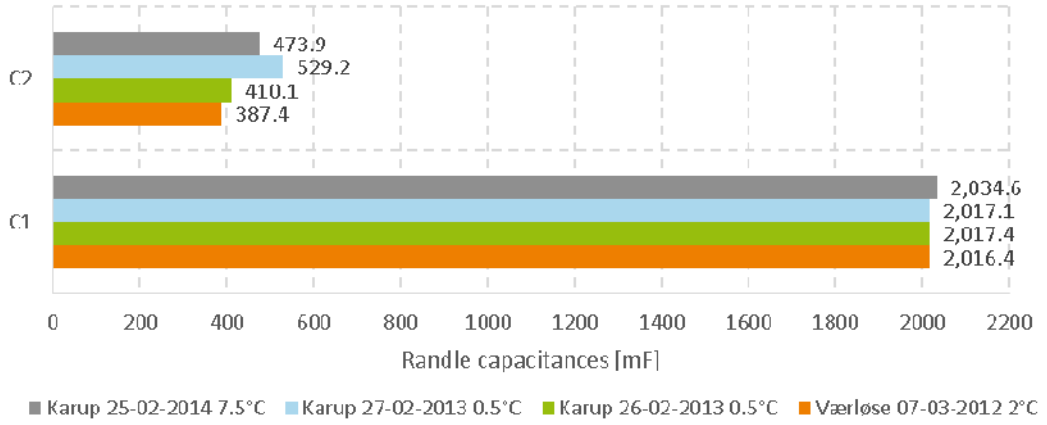

Figure 3.4.21: Randle capacitances for the Mitsubishi i-MiEV batteries used in the on-road tests.

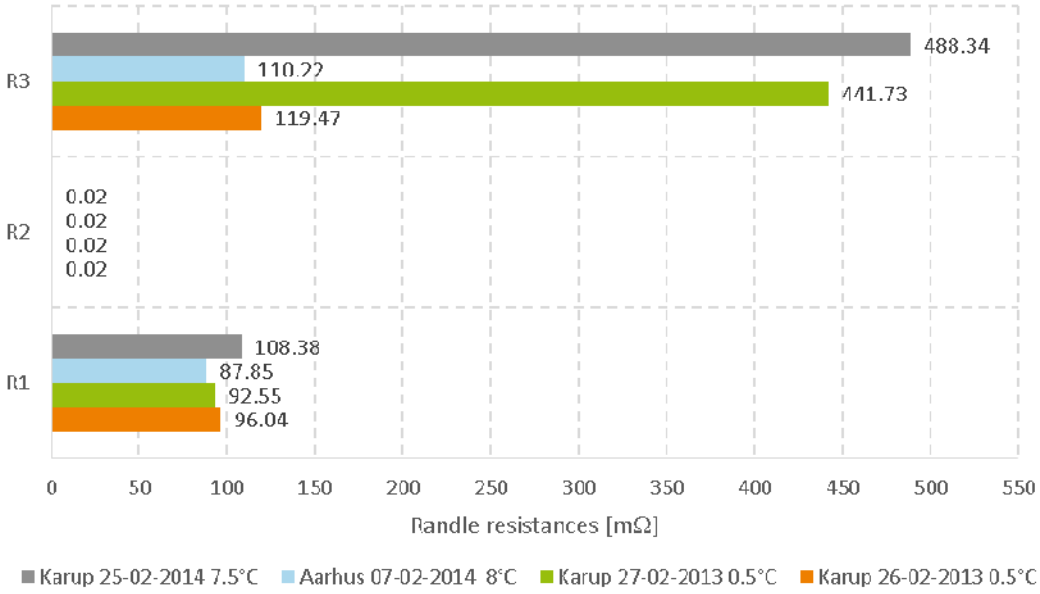

Figure 3.4.22: Randle resistances for the Nissan Leaf batteries[6] used in the on-road tests.

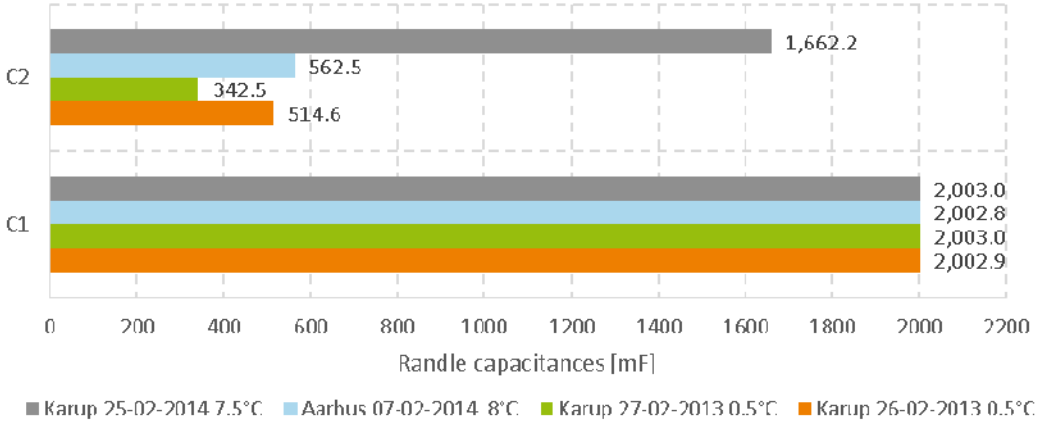

Figure 3.4.23: Randle capacitances for the Nissan Leaf batteries6 used in the on-road tests.

3.5 Experiments versus model

The 2nd order Randle model accurately predicts voltage and voltage drops in both short and long bursts of current. Thus power losses in the battery are predicted well.

Giving a set of data from a full battery discharge cycle produces the most accurate model coefficients. With an EV, a full discharge cycle is limited by the parameters of the vehicle and the battery management

[6] Note that different Nissan Leaf vehicles were tested.

system, which may be more conservative than the manufacturer recommendations. The model is less accurate at highest SOC, depending on the OCV start guess.

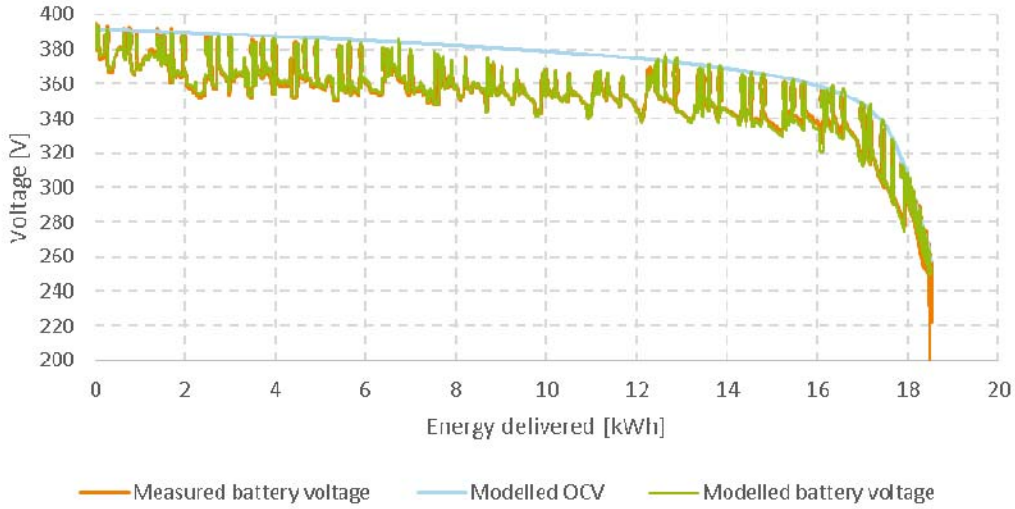

Figure 3.5.1: The modelled OCV and modelled voltage compared to the measured battery voltage, illustrated by the Renault Fluence (25-02-2014 7.5°C).

In Figure 3.5.1 and Figure 3.5.2 shows exemplary plots of the model results – the modelled OCV and modelled battery voltage – compared to the measured battery voltage from which the model coefficients were produced.

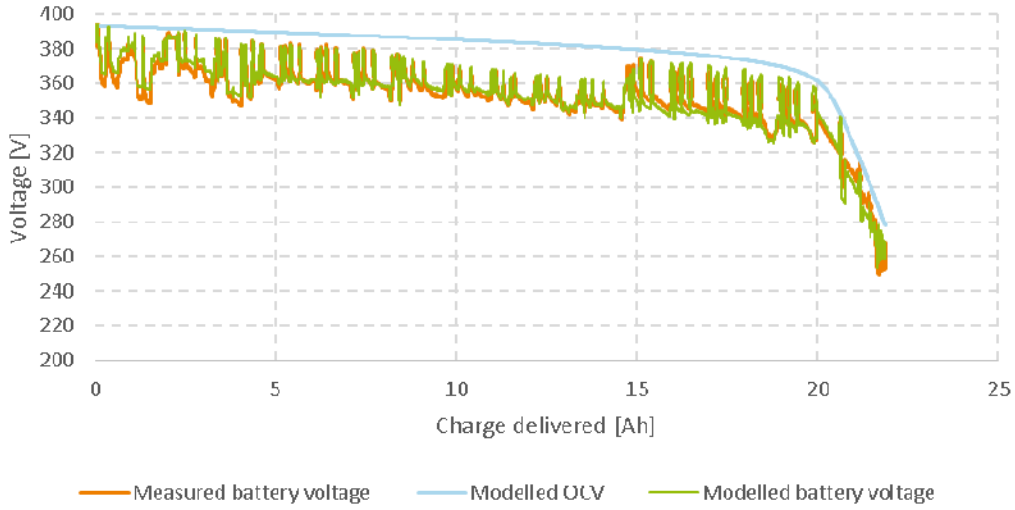

Figure 3.5.2: The modelled OCV and modelled battery voltage compared to the measured battery voltage, illustrated by the Nissan Leaf (25-02-2014 7.5°C).

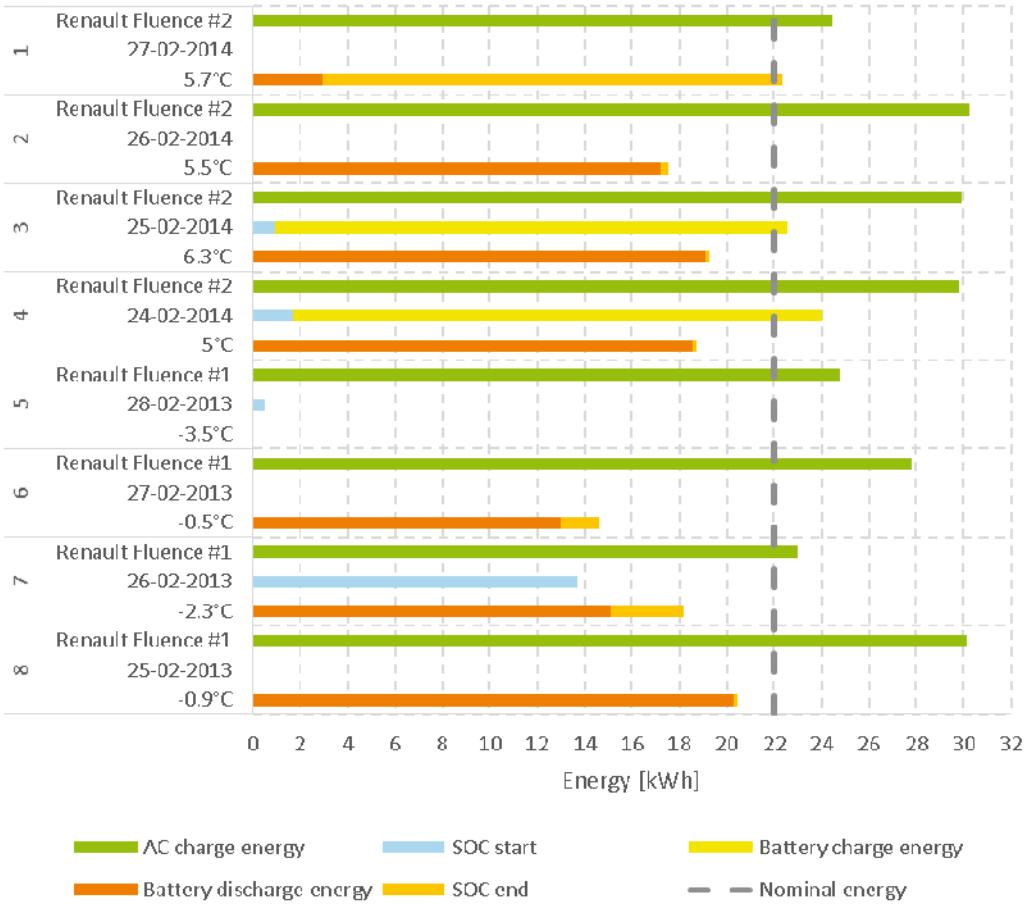

Figure 3.5.3: Energy capacity measurements on the Renault Fluence used in the on-road tests.

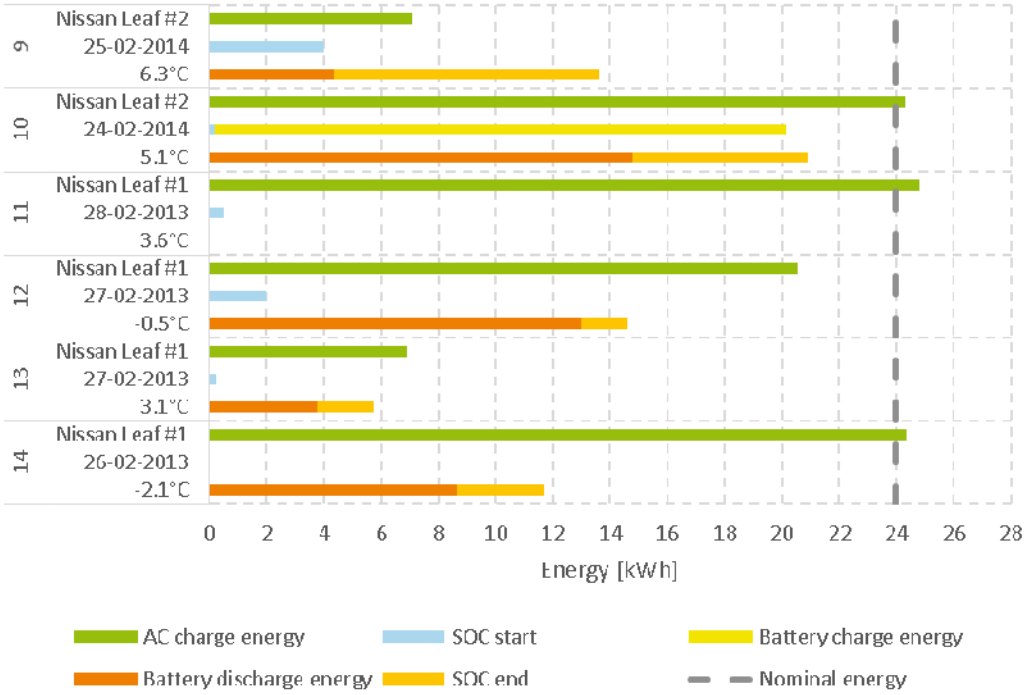

Figure 3.5.4: Energy capacity measurements on the Nissan Leaf used in the on-road tests.

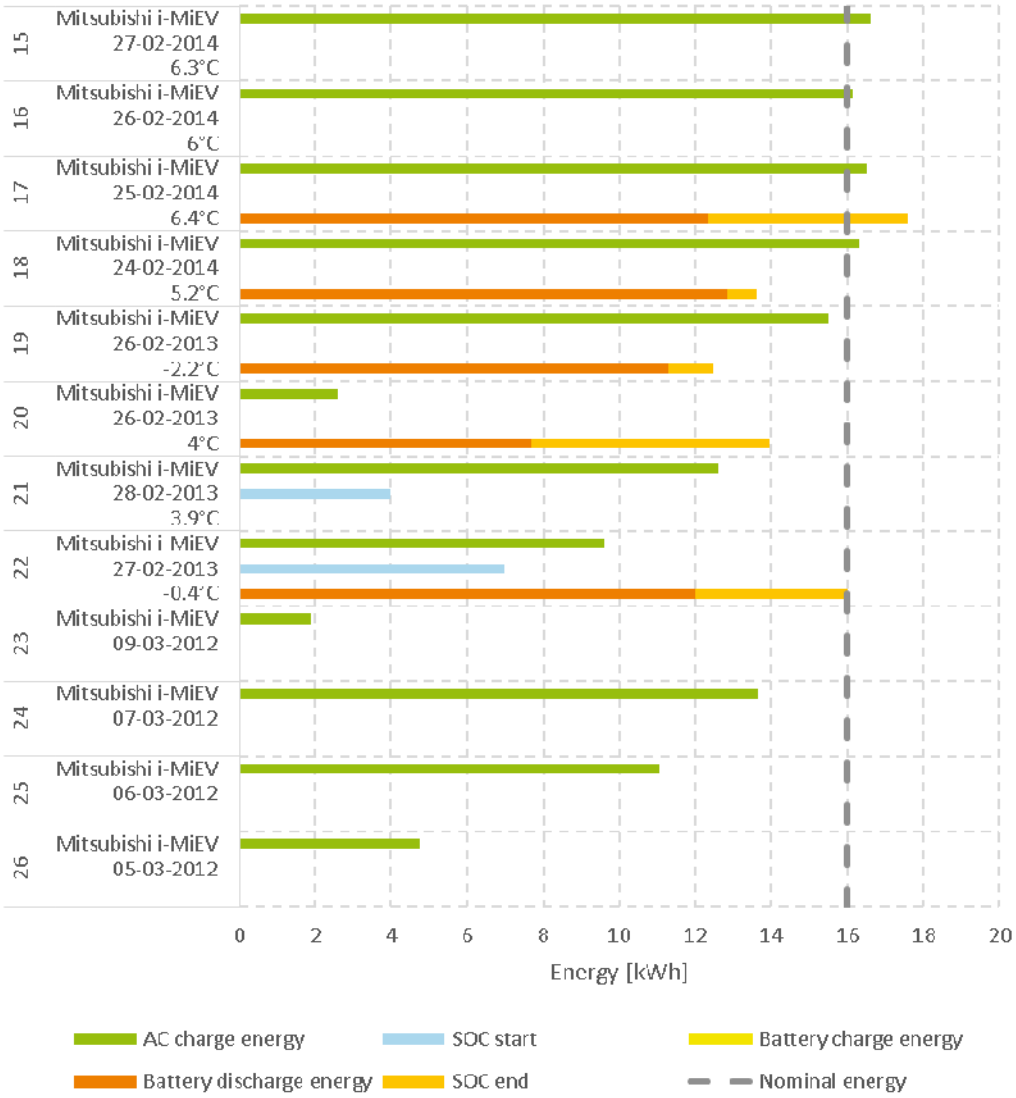

Figure 3.5.5: Energy capacity measurements on the Mitsubishi i-MiEV used in the on-road tests.

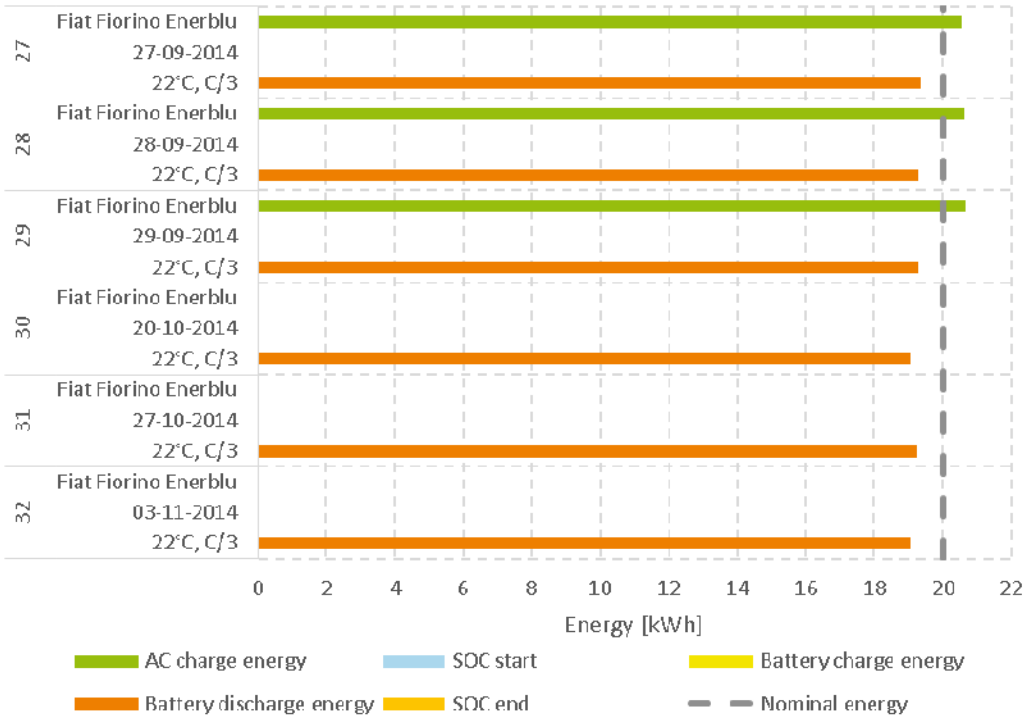

Figure 3.5.6: Energy capacity measurements on the Fiat Fiorino Enerblu measured with the mobile load bank

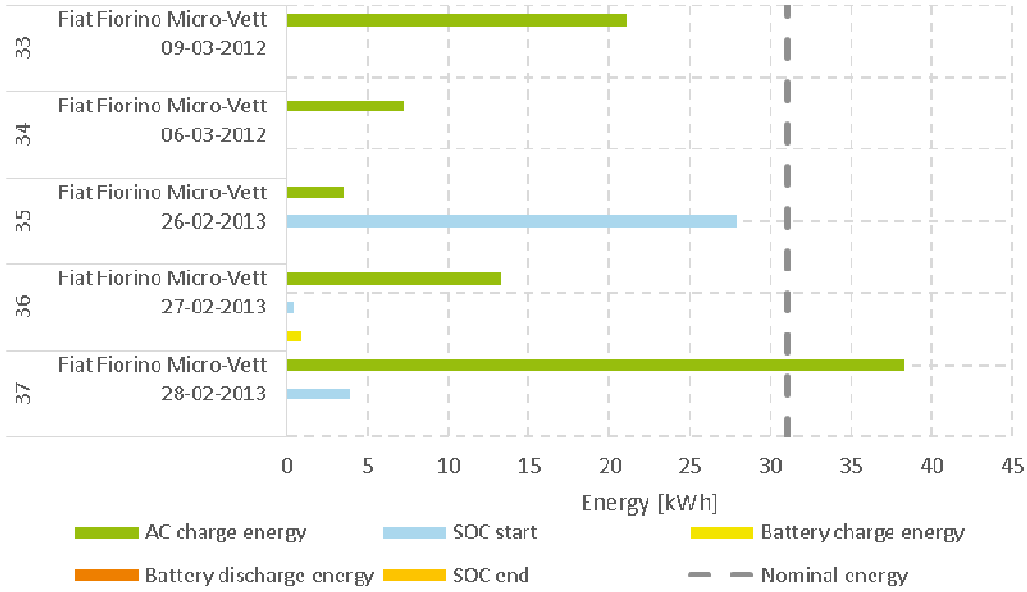

Figure 3.5.7: Energy capacity measurements on the Fiat Fiorino Micro-Vett used in the on-road tests.

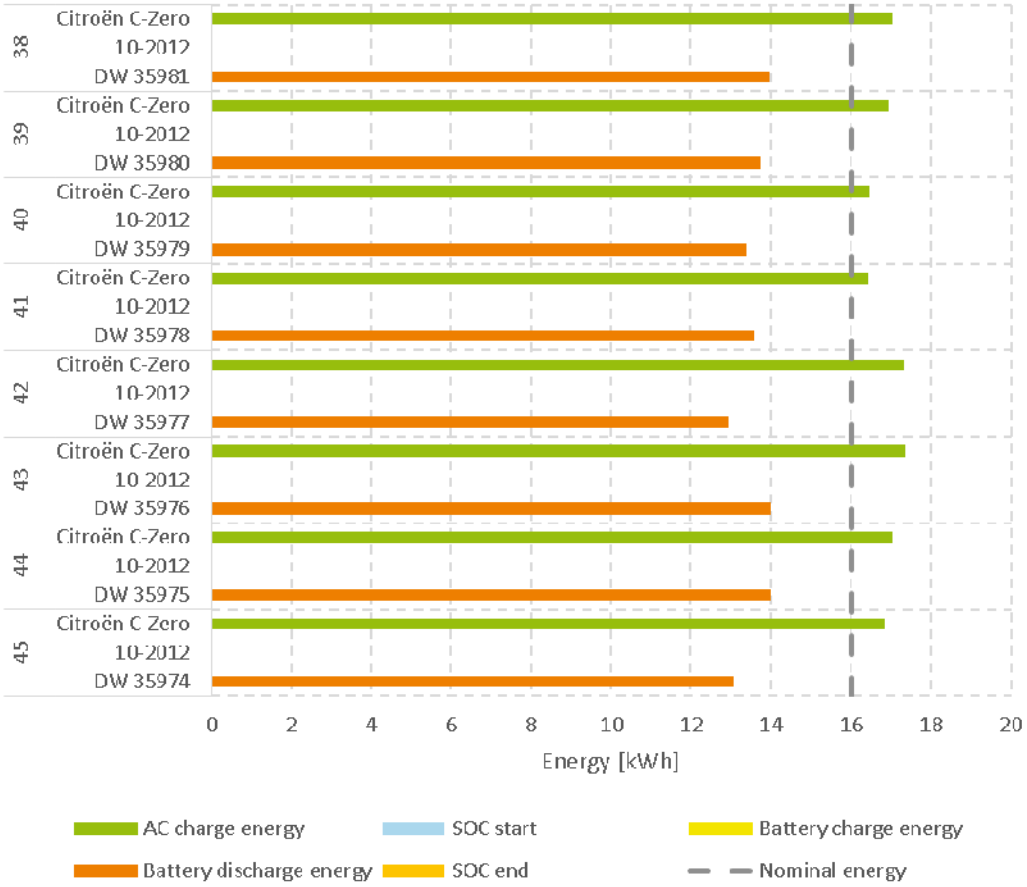

Figure 3.5.8: Energy capacity measurements on eight Citroën C-Zero from the project "Prøv1elbil".

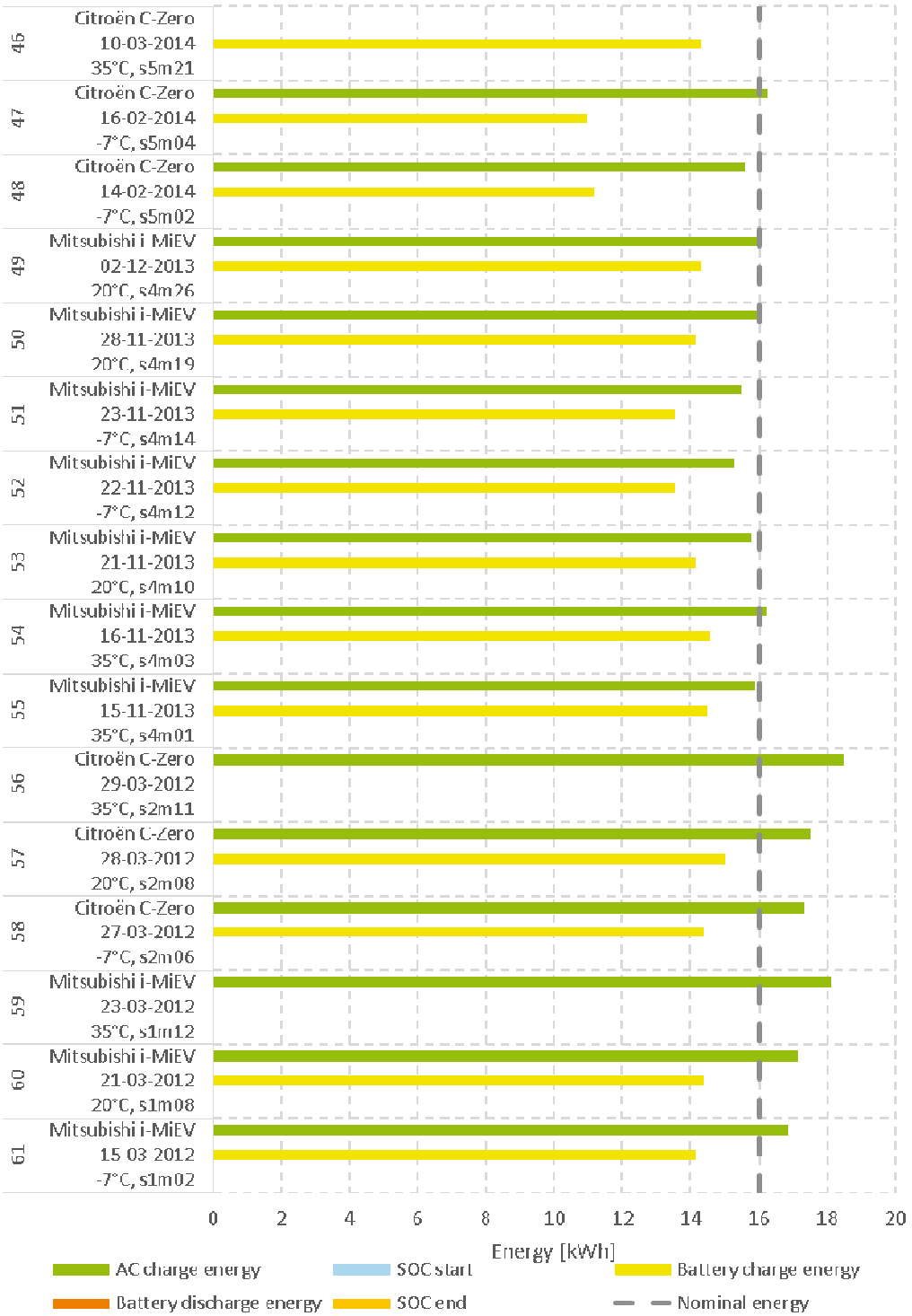

Figure 3.5.9: Energy capacity measurements on Citroën C-Zero and Mitsubishi i-MiEV from TNM

4 Conclusions

The most important part of work presented in this report was to develop a mobile battery and an EV test platform. This has been successfully achieved by building the battery service vehicle, which has proved its worth both in the field and in the laboratory. We have demonstrated that the battery service vehicle is capable of measuring battery capacity in several different ways as well as monitoring internal battery characteristics by reading transient step responses of the battery under fluctuating load.

Due to the restrictions of various control and safety systems on board the vehicles, it has not been possible to separate the battery from the remaining electrical systems of demo vehicles. Furthermore, the current communication protocols do not yet allow bi-directional flow of energy. However, since this will most likely be allowed in the near future through updates to the communication protocols, we demonstrated the possibility of doing capacity and EIS measurements directly on a vehicle. The main part of the measurements was done with the vehicles in normal operation mode without tampering with the battery systems.

The measurements allowed us to use advanced modelling techniques to further investigate the battery characteristics. More specifically it allowed a virtual EIS and ISO12405-2 test to be conducted.

The data did not provide enough evidence to confirm that the battery capacity was actually degrading during the course of this 4-year project. Although the battery management systems on board the vehicles themselves report a decreasing SOH, this could not be translated directly into a measureable loss of capacity. We did however confirm that battery capacity is highly dependent on temperature.

4.1 What can be learned about modelling

The 2^{nd} order Randle circuit performed extremely well at modelling battery current and voltage in short terms.

The battery OCV can be modelled by a rotational symmetric mirrored function of the SOC in AH, based on the normal distribution formula.

From this, we can predict a variety of performance characteristics.

The true SOH of the battery is a composition of its impedance and capacity. The state cannot be revealed during normal driving, but it can be done through analytical methods.

4.2 Why is vehicle power not affected by SOH

Because the internal resistance even in a worn battery pack is relatively low ($<<1\Omega$), there is no real decrease in the current that can be drawn. Therefore the vehicle's acceleration performance is broadly unaffected by changes in battery SOH over its lifetime.

Furthermore, most EVs systems are designed to compensate, by increasing the battery current, when the voltage decreases at low SOC, thus providing a constant vehicle output power. On the other hand, this would decrease the vehicle range as the battery would be discharged faster.

4.3 What are the implications of our findings for policy in general

What this analysis suggests is important to consider when promoting the mass rollout of EVs.

1) The degradation of batteries over time is not as bad as some would suggest
   - Many apparent degradation effects are just temporary effects of temperature
   - Worn batteries can, and should, be repaired rather than replaced

2) Battery capacity and other performance metrics need more attention
   - Capacity needs to be more clearly defined and validated
   - SOC estimates by on board systems need to be improved
   - SOH needs a more clear and uniform definition
   - Battery testing standards should focus on impedance, not just resistance

3) Electric vehicles should be more compatible with standard diagnostics tools
   - Electric vehicles should be using OBD like conventional vehicles
   - Non-intrusive access to batteries for diagnostic purposes should be allowed
   - EIS and similar measurements should be permitted in charging protocols
   - Reverse energy flow should be permitted in charge protocols

4) The impact of temperatures needs to be investigated further
   - Temperature characteristics should be stated by the battery manufacturer
   - Better battery acclimatisation systems should be developed
   - Charging efficiency in cold weather should be improved